



**Aalto University
School of Chemical
Technology**

School of Chemical Technology
Degree Programme of Chemical Technology

Gerard Viader Riera

**INTEGRATED SOLUTION FOR DWTP REVERSE OSMOSIS BRINE
MANAGEMENT: CO₂ STRIPPING FOLLOWED BY MEMBRANE
DISTILLATION**

**Master's thesis for the degree of Master of Science in Technology submitted
for inspection, Espoo, 7 December, 2015.**

Supervisor

Professor Pekka Oinas

Instructors

**Sarwar Golam, D. Sc. (Tech) Aalto University
Edxon Licon, Ph.D.**

Author Gerard Viader Riera

Title of thesis Integrated solution for DWTP Reverse Osmosis brine management: CO₂ stripping followed by Membrane Distillation

Department Biotechnology and chemical technology

Professorship Plant design

Code of professorship KE-107

Thesis supervisor Professor Pekka Oinas

Thesis advisor(s) / Thesis examiner(s) Sarwar Golam, D. Sc. (Tech), Edxon Licon (Ph.D.)

Date 07.12.2015

Number of pages 92

Language English

Abstract

DWTP RO brine disposal options have been studied in this work in terms of technical and economic feasibility. Different pretreatment sequences combining acidification and aeration were carried out and evaluated batchwise in a plate and frame DCMD system at feed and permeate temperatures of 54°C and 21°C respectively. Results showed that acidification provides a simple and inexpensive process in which the initial volume can be reduced by 50% before salts start to precipitate. Aeration followed by acidification provided a volume reduction of 66%, which cannot justify its high OPEX. However, further research in bubbling conditions has the potential to make it a viable process. These pretreatments followed by MD have the potential to become a solid ZLD alternative. Unfortunately, costs derived from brine discharge into the sea are too low to impulse investigation of these technologies

Keywords Reverse Osmosis, Brine, Aeration, Acidification, Membrane Distillation, DCMD

Acknowledgements

First of all I would like to thank Professor Pekka Oinas and specially Sarwar Golam for their support and guidance during the elaboration of this project.

I would like to express my gratitude to Jose Luis Cortina, who gave me the opportunity to write this thesis in Cetaqua; and to Benoît Lefèvre for guiding me throughout my stay in Cetaqua and helping me grow both as a professional and as a person.

I would also like to take this opportunity to thank Ph.D. students from UPC Mònica Reig and Sandra Espriu; and also Oriol Casal for their warm welcome and their indefatigable will to help. Finally, I would like to mention Edxon Licon, one of the most altruistic persons I have ever met, and whose contributions have significantly increased the scientific quality of this thesis. To all of them, many thanks.

I would not like to end this text without expressing my gratitude to my parents and my sisters for being always there.

Table of contents

Abstract	i
Acknowledgements	ii
Table of contents	iii
Nomenclature	v
Abbreviations	vii
List of figures	viii
List of tables	ix
1. Introduction	1
1.1. General introduction	1
1.2. Objective and scope	3
1.3. Structure of the work.	4
Literature part	
2. State of the art.	6
2.1. Membrane distillation	6
2.1.1. History	6
2.1.2. MD configurations	7
2.1.3. Membrane modules	9
2.1.4. Membrane characteristics	10
2.1.5. Heat and mass transfer in DCMD	16
2.1.5.1. Heat transfer	16
2.1.5.2. Mass transfer	20
2.1.6. Fouling	23
2.1.7. Operating parameters	24
2.1.8. MD commercial prototypes	26
2.2. Aeration and acidification.	32

2.2.1. Theoretical principle	33
2.2.2. Mass transfer in aeration	36

Experimental part

3. Materials and methods	40
3.1. Experimental equipment	40
3.2. Experimental procedure	43
3.3. Materials	45
3.4. Experimental design	46
3.5. Analysis.	47
4. Results and discussion	48
4.1. Experimental conditions	48
4.2. Experimental results	50
4.2.1. Aeration	50
4.2.2. MD	52
4.2.2.1. Permeate fluxes	52
4.2.2.2. Evaluation of pretreatments	54
5. Economic pre-feasibility analysis	63
6. Conclusions and recommendations.	71
7. References	73
Appendix I	80

Nomenclature

a	Interphase area (m)
a	Activity coefficient (-)
B	Geometric pore coefficient (-)
C	Concentration (mol/L)
C_M	Membrane coefficient
C_T	Total carbon (mol)
d_e	Collision diameter
h	Heat transfer coefficient ($W \cdot k^{-1} \cdot m^{-2}$)
H	Henry's coefficient ($mol L^{-1} atm^{-1}$)
J	Transmembrane flux ($mol \cdot m^{-2} \cdot s^{-1}$)
k	Thermal conductivity ($W \cdot m^{-1} \cdot k^{-1}$)
K	Mass transfer coefficient (s^{-1})
K_B	Boltzmann constant
Kn	Knudsen number
M_w	Molecular weight of water vapor ($g \cdot mol^{-1}$)
N	Desorption time (min)
P	Pressure (Pa)
q	Heat transfer ($W \cdot m^{-2}$)
r	Mean pore size (nm)
R	Rate of desorption ($mol \cdot s^{-1} \cdot L^{-1}$)
R	Universal gas constant ($8.314 J \cdot K^{-1} \cdot mol^{-1}$)
T	Temperature (K or °C)
V	Volume (L)
X	Mole fraction (-)

Greek letters

ΔH_v	Latent heat of vaporization ($\text{J}\cdot\text{mol}^{-1}$)
γ	Surface tension (J/m^2)
δ	Thickness (μm)
ε	Membrane porosity (%)
θ	Contact angle (rad)
λ	Mean free path (μm)
Φ	Concentration polarization effect (-)
ρ	Density (kg/m^3)
τ	Membrane tortuosity (-)

Subscripts

f	Feed side
g	Gas
l	Liquid
m	Membrane
p	Permeate
pol	Polymer
s	Polymer
w	Water

Abbreviations

AGMD	Air Gap Membrane Distillation
CF	Concentration Factor
DCMD	Direct Contact Membrane Distillation
DGM	Dusty Gas Model
DWTP	Drinking Water Treatment Plant
EDS	Energy Dispersive Spectroscopy
GOR	Gain Output Ratio
ICS	Ion Chromatography System
LEP	Liquid Entry Pressure
MD	Membrane distillation
MED	Multiple-Effect Distillation
MSF	Multi-Stage Flash Distillation
OPEX	Operational Expenditure
PMMA	Poly(methyl methacrylate)
PVDF	Polyvinylidene fluoride
RO	Reverse Osmosis
SEM	Scanning Electron Microscopy
SGMD	Sweeping Gas Membrane Distillation
SJD	Sant Joan Despí
TC	Total Carbon
TIC	Total Inorganic Carbon
TOC	Total Organic Carbon
TPC	Temperature Polarization Coefficient
VMD	Vacuum Membrane Distillation
ZLD	Zero Liquid Discharge

List of figures

1. Milestones in the development of membrane distillation [10]	7
2. Time frame of the works performed on MD process [8]	7
3. Different types of MD configurations [8]	9
4. Heat transfer resistances in the MD system [12]	16
5. Temperature and concentration profile of a DCMD system [12]	17
6. (a) Section of Fraunhofer ISE's spiral wound AGMD module; (b) Picture of the modules [18]	27
7. Concept of the Memstill process based around AGMD [64]	28
8. Scarab AB modules [67]	29
9. Vacuum-Multi-Effect-Membrane-Distillation (V-MEMD) process from Memsys [68]	30
10. Experimental setup of the MD crystallization used by Tun et al. [49]	31
11. Effect of CO ₂ desorption on the pH and on the carbon components distribution [71]	35
12. Carbonic acid dissociation	35
13. Rate of CO ₂ desorption vs. momentary CO ₂ concentration [71]	37
14. Diagram of the MD apparatus	41
15. Diagram of aeration column	43
16. Experimental design scheme	46
17. Aeration of acidified brine (AE1)	50
18. Aeration of raw brine (AE2)	51
19. Distilled water production	53
20. Distilled water production from NaCl solution	54
21. Non-treated brine (MD1)	55
22. Acidified brine (MD2)	56
23. Acidified and aerated brine (MD3)	57
24. Aerated brine (MD4)	58
25. Aerated and acidified brine (MD5)	59
26. Results of SEM/EDS of MD3 (a, b); and MD4 (c, d)	60
27. Concentration Factors (CF)	61
28. Brine disposal options	64

List of tables

1. Characteristic properties of commercial polymer materials commonly used for MD membranes [41]	15
2. Mass transfer mechanisms	21
3. Characteristics of Gas-Liquid Contacting Equipment [72]	38
4. Raw RO brine composition	45
5. Characteristics of membrane	45
6. Experimental conditions of acidification	48
7. Experimental conditions of aeration	48
8. Experimental conditions of MD runs	49
9. Permeate fluxes in MD runs	52
10. Summary of the pretreatment evaluation	61
11. Economic evaluation	69

1. Introduction

1.1 General introduction

In the last decades, scarcity of freshwater resources has led to a significant increase in use of non-conventional water sources. These alternative sources, which include seawater, brackish groundwater and saline wastewater, have been utilized to satisfy the freshwater demand that cannot be met using traditional sources [1], [2]. Growth in use of alternative sources has been bound to the development of technologies able to produce fresh water from highly concentrated saline streams. Main treatment technologies used for this purpose include Reverse Osmosis (RO), Multi-Stage Flash distillation (MSF), Multiple-Effect Distillation (MED), and Electrodialysis (ED) [1].

Among these technologies, RO has been the leading solution for desalination installations, accounting for 60% of the total worldwide installed capacity [1]. In addition to its application for desalination purposes, RO is often found in DWTP (drinking water treatment plants), especially in those cases where source water is obtained from rivers having high salinity levels. RO employs semi-permeable membranes that allow separating a saline solution into two streams: permeate and concentrate [3]. Permeate contains purified water that passes through the membrane, whereas concentrate contains salts and retained compounds. Characteristics of concentrate, also known as brine, depend on many factors, including quality of feed water [3]. Management of RO brines in coastal desalination plants has traditionally been addressed by discharging brine into water bodies, chiefly into the sea. However, the detrimental effect of discharging huge volumes of brine into marine ecosystems, together with its high administrative cost (up to 33% of total cost of desalination [4]), require environmentally friendly options to address the brine management issue [5]. Developing solutions to this problem has become more urgent for inland desalination plants, since the only brine management solutions currently available rely on dilution with other wastewaters, deep well injection, evaporation ponds, or disposal into creeks and ponds. These approaches

provide only partial solutions to mitigate the brine discharge issue. Moreover, they are neither economically nor environmentally sustainable in the long run [6].

Several Zero Liquid Discharge (ZLD) and near-ZLD technologies have shown great promise as a tool to reduce the volume of RO brine, and hence its disposal costs. Today, ZLD technologies are highly desired by manufacturing plants. In addition to the wide public acceptance of the ZLD concept, application of these technologies has been shown to decrease disposal costs and to increase the recovery of fresh water. However, technologies based on the ZLD approach tend to be highly energy-intensive and therefore considered uneconomical [7]. An illustrative example of these energy-intensive technologies would include thermal processes, such as evaporation and evaporative crystallization [3]. Current research has focused on ZLD systems with lower energy requirements. This has intensified interest in Membrane Distillation (MD) technology for brine treatment [8].

MD is a thermally driven membrane process in which the driving force is the transmembrane vapor pressure difference. In this process, vapor molecules are transported through porous hydrophobic membranes from concentrate side to permeate side, in order to achieve separation. The hydrophobic nature of membranes prevents liquid solutions from entering its pores due to surface tension forces [8]. The main advantages that make MD an attractive technology for managing the brine disposal problem include (i) low operating pressure, (ii) not limited by high osmotic pressure constraints, (iii) low sensitivity to feedwater, and (iv) can be supplied by low-grade waste heat from factories or geothermal energy [9].

In spite of all these advantages, MD processes have not reached the industrialization stage yet [10]. The two main technical challenges impeding the industrialization of MD in brine processing are polarization effects as well as fouling and scaling issues. On the one hand, temperature and concentration polarization at membrane interface reduce the effective vapor pressure across the membrane, thus decreasing permeate flux [10]. On the other hand, scaling deposition onto membrane leads as well to a decrease in the permeate flux [11].

A number of brine pretreatments have been developed in order to overcome MD operation problems derived from scaling in the membrane. Usually, these pretreatments rely either on causing dissolved salts to precipitate prior to MD or on delaying the precipitation of those salts. Those pretreatments that rely on removal of salts provide feeds for MD that can be highly concentrated without having scale formation. However, since the mechanism is based

on the precipitation of salts, a filtration step is required. On the other hand, those pretreatments that delay salts precipitation usually require of the addition of chemical products such as antiscalant.

Aeration and acidification are novel pretreatments for RO brine having high carbonate content. Aeration, also known as CO₂ stripping is a technique based on removal of carbonates in form of CO₂. This technique consists in bubbling air through a column of brackish water. As air bubbles rise through the column, dissolved CO₂ is transported from bulk water to bubbles, reducing thus the content of carbonate in water. Since the transport of CO₂ is highly affected by the pH of the solution, aeration is usually carried out in combination with acidification in order to achieve maximum CO₂ removal. Acidification can also be applied as a pretreatment technique by itself. By acidifying, the equilibrium of the carbonate system is modified, drastically reducing the presence of CO₃²⁻. Decreasing the concentration of CO₃²⁻, the precipitation of CaCO₃ can be significantly diminished.

1.2 Objective and scope

The main objective of this thesis is to assess the technical and economic feasibility of solving the RO brine problem of a DWTP by applying a pretreatment stage consisting in aeration and or acidification followed by MD. The disposal of RO in Sant Joan Despí DWTP (Barcelona) was considered a particular case study throughout the work. Details of Sant Joan Despí DWTP are presented in appendix 1.

The secondary objective is to experimentally study aeration, acidification, and their combination as a pretreatment for RO brine, and to identify which is the most effective technique for scale inhibition in MD

1.3 Structure of the work

In order to achieve the above-mentioned objectives, an extensive literature review and an experimental study on MD technology and brine pretreatments were carried out. The work structure can then be divided in two parts; the literature part (chapter 2) and the experimental part (chapters 3, 4, 5, 6).

In chapter 2, the MD technology is presented, paying special attention to MD configurations, membrane modules and characteristics, heat and mass transfer through the membrane, fouling, and effect of operating parameter on the process efficiency. In addition, chapter 1 includes a state of the art of the most significant MD commercial prototypes. Finally, the theoretical principles behind aeration and acidification are reported for a better understanding of these pretreatment techniques.

An extensive description of the experimental research can be found in chapter 3. This chapter is centered in the equipment used, experimental procedure, materials, and experimental planning. Parameters that were analyzed and techniques used are also described in chapter 3.

All the results and important data of the experimental study are presented and briefly described in chapter 4. Besides showing the results, this chapter includes a thorough analysis and a discussion of the experiments main outcomes.

In chapter 5, economic feasibility of pretreating RO brine and reducing its discharge through MD is evaluated. Finally, conclusions and recommendations for further studies can be found in chapter 6.

LITERATURE PART

2. State of the art

2.1. Membrane distillation

In this section the most significant details of MD technology are presented. The sections composing this chapter include: history, MD configurations, types of membrane modules, membrane characteristics, heat and mass transfer, fouling, operating parameters, and a state of the art of the most significant MD commercial prototypes.

2.1.1. History

The first investigations about MD process can be traced back to Bodell and Wehl [10]. In their initial approach, Bodell and Wehl presented MD as an alternative process for desalination of saline water. The investigations on this technology resulted in the first patent on MD, published by Wehl in 1963. However, interest on MD faded quickly due to its lower production compared to RO technique, which had been triggered by the development of high flux asymmetric cellulose acetate membranes [8], [10]. This lack of interest led to a “death” phase of MD in which no reported study on MD can be found.

By the 1980s, interest in MD was recovered within the academic communities as novel membranes and modules with better characteristics became available [8]. In the following years, the perception of MD as a promising technique grew among the scientific community, which became aware of the benefits of a separation technology that could be run on low-grade heat waste or alternative energy sources [8]. In the 1985s the first efforts to commercialize MD were made by Gore and Associates (USA), Enka AG (Germany) and the Swedish Development Co. Unfortunately, results showed that MD had not been commercially accepted as a feasible process [10].

From that time on, there has been a vast growing interest in MD. However, from a commercial standpoint, MD is not implemented yet in industry [8], [10]. The evolution of the MD process is illustrated in Figure 1 and Figure 2. On one hand, Figure 1 presents a timeline

of the main phases and milestones of MD development. On the other hand, Figure 2 presents the time frame of the works performed on MD since its first appearance.

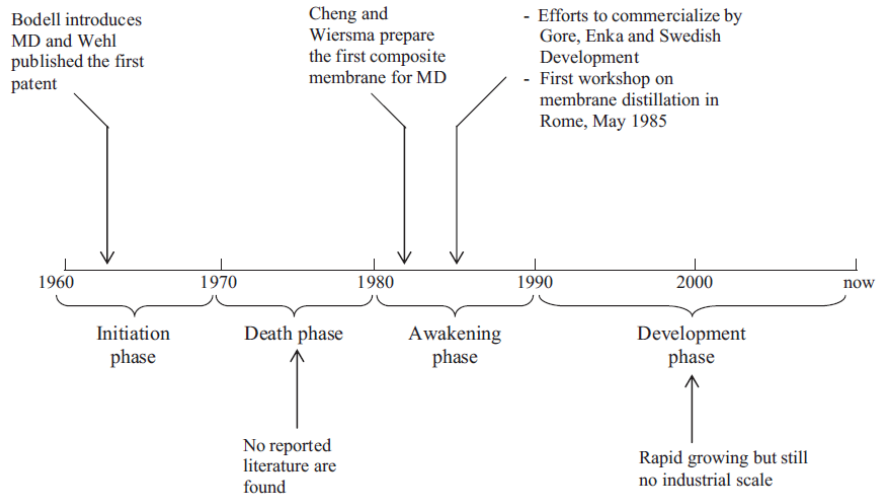


Figure 1. Milestones in the development of membrane distillation [10]

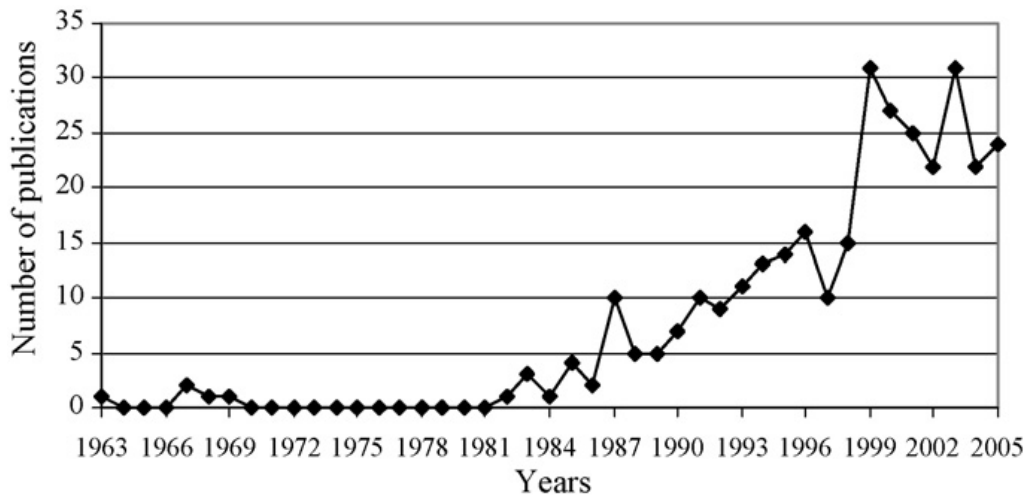


Figure 2. Time frame of the works performed on MD process [8]

2.1.2. MD configurations

In this section the four possible configurations that MD systems can take are described together with their advantages, disadvantages, and suitable applications. These configurations

differ from each other in the medium in contact with the membrane at the permeate side. A schematic representation of the four configurations is presented in Figure 3.

i. Direct Contact Membrane Distillation (DCMD)

In DCMD the membrane is in direct contact with both liquid phases (feed and permeate). This is the simplest configuration and is capable of producing reasonable high flux despite its high heat lost by conduction. It is best suited for applications such as desalination and concentration of aqueous solutions (e.g., juice concentrates) [1].

ii. Air Gap Membrane Distillation (AGMD)

In AGMD an air gap is interposed between the membrane and the condensation surface. This configuration has the highest energy efficiency due to reduced heat lost by conduction. However, the flux obtained is generally low due to low temperature difference across the membrane and therefore larger surface areas are required [1]. The AGMD configuration can be widely employed for most MD applications, particularly where energy availability is low or in those cases where volatile compounds need to be removed from aqueous solutions [12].

iii. Sweeping Gas Membrane Distillation (SGMD)

In SGMD a stripping inert gas is used at the permeate side to carry the vapor to condense outside the membrane module. Similarly to AGMD, this configuration uses a gas barrier to reduce heat loss. However, in this case the gas is not stationary, which enhances the mass transfer coefficient. In this technique, the vapor diffuses in the stripping gas as it is swept. This results in a need for a large condenser, which represents the main disadvantage of this configuration [12]. Furthermore, an air blower or a compressor are needed to maintain operation of this configuration, which causes an increase in both CAPEX and OPEX. SGMD configuration is suited for solutions containing volatile compounds [12].

iv. Vacuum Membrane Distillation (VMD)

In VMD the permeate side is vapor or air under vacuum conditions. This configuration makes the heat lost conduction negligible and allows for condensation outside the membrane module. VMD is used to separate volatiles from aqueous solution [12].

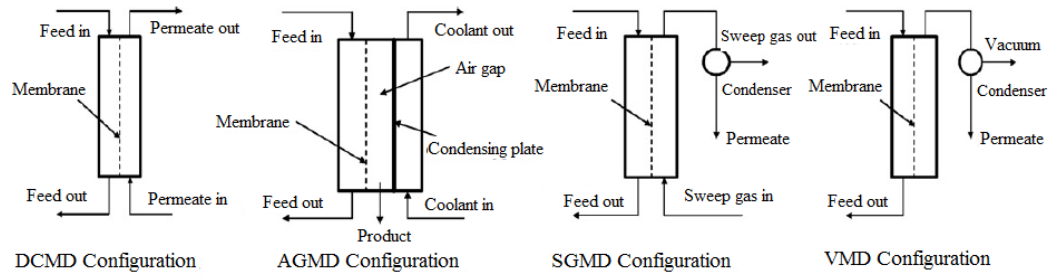


Figure 3. Different types of MD configurations [8]

Among the four configurations, DCMD is the most popular for laboratory research due to its easy set up and operation [1]. However, AGMD is more popular in commercial applications due to its higher energy efficiency and capability for latent heat recovery [1].

2.1.3. Membrane modules

Design of MD modules must permit high feed and permeate flow rates with high turbulence and low pressure drop along the membrane module. In addition, due to the non-isothermal nature of MD modules, they must also guarantee a good heat recovery function and thermal stability [8].

Three major MD module configurations have been developed: (i) plate and frame, (ii) tubular, and (iii) spiral wound. The two former have been widely used in pilot plant trials [1], whereas the latter has been focused toward industrial applications. These module configurations are merely the support for the membrane, which has to be adequate for each configuration; plate and frame, and spiral wound configurations are assembled using flat sheet membranes, while tubular configuration requires hollow fiber membranes.

i. Plate and frame

Plate and frame configuration can be operated in any of the four MD configurations. In this configuration, the packing density is about $100\text{-}400\text{ m}^2/\text{m}^3$ [13],[14]. This module is widely employed in laboratory experiments due to the fact that it is easy to construct and broken membranes can be easily replaced [14].

ii. Tubular

Tubular configuration consists of thousands of hollow fiber membranes bundled and sealed inside a shell tube [12]. This module can have packing densities as high as $3000 \text{ m}^2/\text{m}^3$ [14], [15]. In this configuration the feed is introduced into the shell side or into the lumen side of the hollow fibers, and cooling fluid, sweeping gas, or negative pressure can be applied on the other side to form DCMD, SGMD, or VMD respectively. Because of its large active area, this configuration has a great potential in commercial applications [14]. The main disadvantage of this configuration is that good flow distribution on the shell side might be difficult to achieve, with subsequent high degrees of temperature polarization. Nevertheless, flow distribution might be enhanced in cross-flow modules. Another disadvantage of tubular modules is the high tendency to fouling and the difficulty to clean and maintain [12]. Furthermore, if feed solution penetrates the membrane pores the whole module must be changed [14], [16].

iii. Spiral wound

Spiral wound configuration has been developed in order to meet the requirements of commercial applications. These modules are mainly employed in AGMD regime, and have much more compact structure than the conventional plate and frame modules [17], [18]. In this configuration, flat sheet membranes and spacers are enveloped and rolled around a perforated central collecting tube [12]. Feed moves across the membrane surface in an axial direction, while the permeate flows radially to the center and exits through the collection tube [12]. Spiral wound membrane has good packing density, average tendency to fouling and acceptable energy consumption [16].

2.1.4. Membrane characteristics

In comparison to other membrane separation processes, only few authors have considered the possibility of designing membranes for MD. As a result, most of the membranes used for MD purposes are actually hydrophobic membranes made for microfiltration purposes [8].

In this section the most significant parameters affecting the transmembrane flux are presented. These parameters are the mean pore size (r), membrane thickness (δ_m), membrane porosity

(ε), and membrane tortuosity (τ) [8]. The relationship between these parameters and the transmembrane flux (J) is described as follows, where a is a factor whose value equals 1 or 2 for Knudsen diffusion and viscous fluxes, respectively [19].

$$J \propto \frac{r^a \varepsilon}{\delta_m \tau} \quad (1)$$

Besides the abovementioned parameters, the thermal conductivity (k_m), surface chemistry, liquid entry pressure (LEP), and membrane material need to be taken into account when designing a MD system. These parameters are detailed as well in this section.

i. Mean pore size (r) and pore size distribution

A large pore size is required for high permeate flux, while pore size should be small to avoid liquid penetration. As a result, optimum pore size should be determined for each feed solution and operating condition [12]. Membranes used in MD systems usually have pore sizes ranging from 100 nm to 1 μm [8], [19].

Membranes employed in MD systems exhibit a pore size distribution rather than a uniform pore size [8]. Therefore, more than one mechanism can take place simultaneously depending on the pore size and on the MD operating conditions.

ii. Membrane thickness (δ_m)

Membrane thickness is a significant characteristic in MD systems. As the membrane becomes thicker the mass and heat transfer resistances increase. On one hand, increase of the mass transfer resistance leads to a reduction of the permeate flux. On the other hand, an increase of the heat transfer surface results in a higher thermal efficiency of the system [12]. According to [20], the optimum membrane thickness lies between 30-60 μm .

iii. Membrane porosity (ε)

Membrane porosity refers to the void volume fraction of the membrane (defined as the volume of pores divided by the total volume of the membrane). In general MD membrane

porosity lies between 30 and 85% [8]. Membranes having high porosity have larger evaporation surface areas, which result in higher permeate fluxes and lower conductive heat losses. The Smolder-Franken equation for the determination of the porosity (ε) is presented as follows [21].

$$\varepsilon = 1 - \frac{\rho_m}{\rho_{pol}} \quad (2)$$

where ρ_m and ρ_{pol} are the densities of membrane and polymer material, respectively.

iv. Membrane tortuosity (τ)

Membrane tortuosity is the average length of the pore compared to the membrane thickness [8]. The higher the tortuosity value, the lower the permeate flux. This is due to the fact that diffusing molecules must move along tortuous paths. Due to difficulties in measuring the real value of tortuosity for the microporous membranes used in MD process, investigators frequently assume it as a correction factor [22]–[24]. A correlation between tortuosity and porosity developed by [25] is presented as follows

$$\tau = \frac{(2 - \varepsilon)^2}{\varepsilon} \quad (3)$$

v. Thermal conductivity (k_m)

Thermal conductivity of the membrane is calculated based on thermal conductivity of both polymer (k_s) and fluid in the pores (k_g), which is usually air. This calculation uses a volume-average of both conductivities.

$$k_m = (1 - \varepsilon)k_s + \varepsilon k_g \quad (4)$$

On one hand, the thermal conductivity of the polymer depends on the temperature, the degree of crystallinity, and the shape of the crystal [12]. On the other hand, thermal conductivity of water vapor and air at around 40°C can be calculated as follows [26].

$$k_g = 1.5 \times 10^{-3} \sqrt{T} \quad (5)$$

vi. Membrane surface chemistry

Hydrophobicity can be achieved either by using hydrophobic materials such as PTFE, PVDF, PP, and PE; or by making the membrane surface energy as low as possible by means of different surface modification techniques of hydrophilic membranes [27]–[31]. These techniques involve a highly water permeable plasma polymerization coating of silicon fluoropolymer layer on the outside surface of porous hydrophobic membranes (PP fibers). The layer is extremely thin, porous and covers the entire surface to create a patchy layer of hydrophobic microporous/porous coating on the surface of hydrophobic porous membranes [32], [33].

vii. Liquid Entry Pressure (LEP)

LEP or wetting pressure is a characteristic of the membrane that indicates which is the maximum pressure that the membrane is able to withstand without suffering pore wetting. When a membrane suffers pore wetting, i.e. feed liquid penetrates membrane pores, the membranes loses its hydrophobicity and lets feed water through. LEP depends on maximum pore size and membrane hydrophobicity [12]. However, it is also affected by feed concentration and presence of organic solutes, which usually reduce LEP [34]. According to Franken et al. [35], LEP can be estimated as follows

$$\Delta P = P_f - P_p = \frac{-2B\gamma_l \cos\theta}{r_{max}} \quad (6)$$


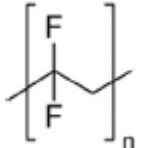
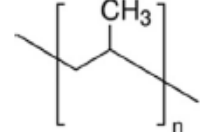
where P_f and P_p are the hydraulic pressure on the feed and permeate side, B is a geometric pore coefficient (equal to 1 for cylindrical pores), γ_l is liquid surface tension, θ contact angle and r_{max} is the maximum pore size.

viii. Membrane materials

The most common materials used for MD membranes are PTFE, PVDF and PP [36]. PTFE has the highest hydrophobicity as well as good chemical and thermal stability, and oxidation resistance. However, it has the highest thermal conductivity, which will cause greater heat transfer through the membrane and hence high heat losses by conduction. PVDF is not as hydrophobic as PTFE; nevertheless, it has good thermal resistance and mechanical strength. PVDF can be easily prepared into membranes with versatile pore structures by different methods [14]. PP provides the lowest thermal conductivity among these three materials. Furthermore, it exhibits good thermal and chemical resistance [14]. Properties of commercial materials commonly used for MD membranes are presented in Table 1.

Recently, new membranes materials with good mechanical strength as well as high hydrophobicity and porosity have been developed. These new materials include carbon nanotubes, fluorinated copolymer materials and surface modified PES [37]–[40].

Table 1. Characteristic properties of commercial polymer materials commonly used for MD membranes [41]

Polymer materials	Chemical structure	Surface energy ($\times 10^{-3} \text{ N m}^{-1}$)	Thermal conductivity ($\text{W m}^{-1} \text{ K}^{-1}$)	Thermal stability	Chemical stability	Fabrication method
PTFE		9-20	0.25	Good	Good	Sintering Melt-extrusion
PVDF		30.3	0.19	Moderate	Good	NIPS TIPS Electro-spinning
PP		30	0.17	Moderate	Good	Melt-extrusion TIPS

2.1.5. Heat and mass transfer in DCMD

This section presents the principles behind mass and heat transfer in DCMD. The objective of this section is to provide an overview of the transport phenomena and how these are affected by different operational parameters.

2.1.5.1. Heat transfer

Heat transfer is believed to be the rate controlling step in the DCMD process, and occurs in four different manners [8]:

- Heat transfer by convection from feed solution to the membrane surface across the unstirred boundary layer in the feed side of the membrane module (related to the temperature polarization effect).
- Heat transport by conduction across both the membrane matrix and the gas filled pores (considered heat loss in MD).
- Heat associated to latent heat of vaporization and therefore to the mass transfer through the membrane pores (efficient heat in MD).
- Heat transfer by convection from the membrane surface to the permeate solution across the boundary layer in the permeate side.

The scheme of these heat transfer steps and the corresponding temperature profile are presented respectively in Figure 4 and Figure 5.

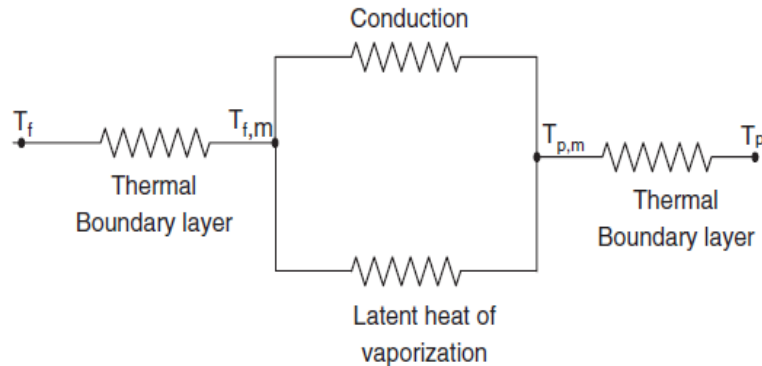


Figure 4. Heat transfer resistances in the MD system [12]

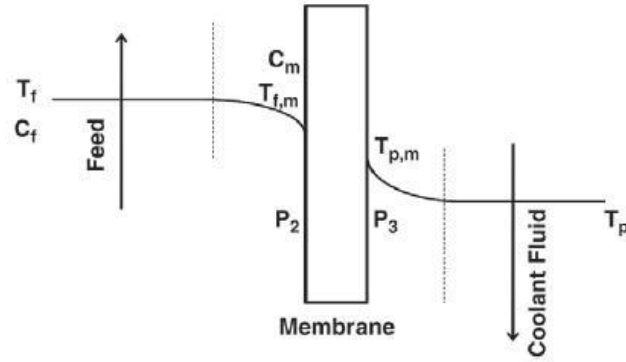


Figure 5. Temperature and concentration profile of a DCMD system [12]

- i. Heat transfer by convection through feed and permeate sides boundary layers (a & d)

The heat transfer boundary layer formed at each side of the membrane surface imposes a resistance to heat transfer and makes the temperature difference at the liquid/membrane interfaces lower than that applied at the bulk phases. This phenomenon, known as temperature polarization, affects negatively the driving force for mass transfer [8]. The temperature polarization coefficient (TPC) describes the fraction of transmembrane temperature to bulk temperature difference as shown as follows [8]

$$TPC = \frac{T_{fm} - T_{pm}}{T_f - T_p} \quad (7)$$

where T_{fm} , T_{pm} , T_f and T_p are membrane surface temperatures and fluid bulk temperatures at the feed and the permeate side, respectively.

Figure 5 shows that due to the temperature polarization effects, the bulk feed temperature T_f gradually decreases across the developed boundary layer to T_{fm} , which is the feed temperature at the membrane surface. Similarly, at the permeate side, the temperature at the membrane surface (T_{pm}) is higher than that of the permeate bulk phase (T_p) due to the developed permeate boundary. Both feed and permeate boundary layers are function of fluid

properties and operating conditions, as well as hydrodynamic conditions. It is convenient to work under optimum mixing conditions to diminish the temperature polarization effects [8].

Heat transfer by convection in the feed (q_f) and permeate (q_p) boundary layer can be calculated as shown in the following equations.

$$q_f = h_f(T_f - T_{fm}) \quad (8)$$

$$q_p = h_p(T_{pm} - T_p) \quad (9)$$

where h_f and h_p are the film heat transfer coefficient of the boundary layer for the feed and the permeate side respectively [8].

ii. Heat transport by conduction through the membrane (b)

In MD, the fraction of heat transferred by conduction through both the membrane matrix and the gas filled pores is considered heat lost and should be minimized in order to decrease the temperature polarization effect and increase efficiency of the MD process. Heat transferred by conduction through the membrane can be calculated as follows [8].

$$q_m = h_m(T_{fm} - T_{pm}) \quad (10)$$

where h_m is the heat transfer coefficient, which can be evaluated as

$$h_m = \frac{k_m}{\delta_m} \quad (11)$$

where δ_m is the thickness of the membrane and k_m is the average thermal conductivity of the membrane (Equation (4)) [8].

iii. Heat transfer by movement of vapor across the membrane (c)

The amount of heat that contributes to water evaporation is considered the efficient heat. Efficiency of the MD process is maximized when temperature polarization effect, internal heat lost by conduction through the membrane, and external heat lost to the environment are reduced. The efficient heat can be estimated as follows [8].

$$q_v = J\Delta H_v \quad (12)$$

where J is the MD molar flux and ΔH_v is the latent heat of vaporization.

The total heat transferred through the membrane whether it is considered efficient heat or heat lost by conduction may be calculated as follows.

$$q_{m+v} = q_m + q_v = h_m(T_{fm} - T_{pm}) + J\Delta H_v \quad (13)$$

It is important to note as well that under steady state conditions, overall heat transfer flux through the membrane is given by the following equation[8].

$$q_f = q_{m+v} = q_p \quad (14)$$

2.1.5.2. Mass transfer

The mechanism through which brine is concentrated, and distilled water produced in DCMD can be described in three stages. Firstly, hot feed vaporizes from the liquid/gas interface (pore entrance). Secondly vapor is driven by the vapor pressure difference and crosses from the hot interface to the cold interface through the pores. Finally, in the third stage, vapor condenses into the cold side stream [42]. From this mechanism, it can be observed that the two major factors controlling mass transfer are (i) vapor pressure difference (driving force), and (ii) the permeability of the membrane (resistance) [1].

Mass transfer across the pore membranes is usually described with the Dusty Gas Model (DGM) [25]. The Dusty gas model elucidates mass transfer in porous media by four possible mechanisms: viscous flow, Knudsen diffusion, molecular diffusion, and surface diffusion. Among these four mechanisms, surface diffusion and viscous flow are commonly neglected [19].

The active mechanism in mass transfer inside the membrane pore can be estimated using the Knudsen number (Kn), which can be expressed as the ratio of mean free path (λ) of transported molecules to the membrane pore size (d_p) as shown in the following equation [43].

$$Kn = \lambda/d_p \quad (15)$$

The mean free path can be described as the average distance travelled by molecules to make collisions (λ). This parameter can be calculated as follows.

$$\lambda = \frac{k_B T}{\sqrt{2} \pi P d_e^2} \quad (16)$$

where k_B , T and P are Boltzman constant, absolute temperature, and average pressure within the membrane pores respectively. The symbol d_e represents the collision diameter for water vapor (2.64×10^{-10}) and air (3.66×10^{-10}) molecules [12]. The mean free path value of water vapor at 60°C was estimated to be 0.11 μm [44].

The mass transfer mechanisms are described in Table 2 together with their condition and membrane coefficient equation.

Table 2. Mass transfer mechanisms

Mechanism	Condition	Description	Membrane coefficient	Reference
Knudsen diffusion	$Kn > 1$	The mean free path of water vapor molecules is large compared to the membrane pore size, which means the molecule-pore wall collisions are dominant over molecule-molecule collisions	$C_m = \frac{2\pi}{3} \frac{1}{RT} \left(\frac{8RT}{\pi M_w} \right)^{1/2} \frac{r^3}{\tau \delta}$	[23]
Molecular diffusion	$Kn < 0.01$	The vapor flux diffuses through stationary air film (the air which exists inside the membrane pores)	$C_m = \frac{\pi}{RT} \frac{PD}{P_{air}} \frac{r^2}{\tau \delta}$	[12]
Transition diffusion	$0.01 < Kn < 1$	The water vapor molecules collide with each other, and also diffuse through air film. Consequently, the mass transfer takes place by both the Knudse/ordinary diffusion mechanism.	$C_m = \frac{\pi}{RT} \frac{1}{\tau \delta} \left[\left(\frac{2}{3} \left(\frac{8RT}{\pi M_w} \right)^{1/2} r^3 \right)^{-1} + \left(\frac{PD}{P_{air}} r^2 \right)^{-1} \right]^{-1}$	[23]

where ε , τ , r , δ , M_w , P and P_{air} are porosity, pore tortuosity, pore radius, membrane thickness, molecular weight of water vapor, total pressure inside the pore, and air pressure within the membrane pore respectively.

Regardless of the particular active mechanism, mass flux can be expressed as shown in the following equation

$$J = C_m(P_{fm} - P_{pm}) \quad (17)$$

where P_{fm} and P_{pm} are vapor pressure at membrane feed and permeate surfaces respectively, and C_m is the membrane coefficient. Vapor pressure can be found from Antoine equation, whereas membrane coefficient for each mechanism can be obtained from Table 2.

Vapor pressure at feed side of the membrane is affected by concentration of salts (the higher the concentration the lower the vapor pressure). This decrease in vapor pressure negatively affects the efficiency of those MD systems in which high concentrations of salts are to be achieved. For non-ideal binary mixtures, the partial pressure can be calculated as follows [45].

$$p_1 = X_w a_w P_w \quad (18)$$

where X_w is the liquid mole fraction of water and P_w is the vapor pressure of the deionized water as given by Antoine equation. The water activity (a_w) for a binary NaCl solution can be defined as shown in the following equation.

$$a_w = 1 - 0.5x - 10x_{NaCl}^2 \quad (19)$$

where x_{NaCl} is the mole fraction of NaCl in the solution [46].

Similarly to temperature polarization, concentration polarization can also occur in DCMD. This phenomenon is caused by the evaporation of water at the liquid/gas interface (membrane pores), and results in a boundary layer having higher concentration than the bulk solution. The concentration polarization coefficient (Φ) can be expressed as follows.

$$\Phi = \frac{C_{fm}}{C_f} \quad (20)$$

where C_{fm} and C_f are the concentration at the membrane and at the bulk solution respectively (Figure 5). Concentration at the membrane can be estimated using the relation from the following equation [12]

$$C_{fm} = C_f \exp\left(\frac{j}{\rho K}\right) \quad (21)$$

where ρ is the liquid density and K is the mass transfer coefficient.

The effect of concentration polarization can be decreased by increasing turbulence on the membrane surface.

2.1.6. Fouling

Fouling is one of the main concerns in operation of MD systems, being especially significant in those cases that involve highly concentrated salt solutions. Fouling phenomena consists in deposition and buildup of undesirable materials on membrane surface and membrane pores, which may reduce permeate flux and process efficiency by decreasing the overall heat transfer coefficient [12]. This deposited undesirable layer may be formed by (i) crystalline deposits, (ii) biological growth, or (iii) suspended particles and corrosion products [8].

i. Crystallization fouling

Crystallization fouling, also known as scaling, results from deposition and growth of crystals on membrane surfaces during the treatment of salt concentrated feed solutions [47]. Scaling is one of the major problems in MD processes involving highly concentrated brines [47]. Shirazi et al. [48] pointed out that membrane fouling by inorganic salt depends on the membrane properties, module geometry, feed solution characteristics, type of salt, and operating conditions.

Tun et al. [49] studied the effect of high concentration of NaCl and Na₂SO₄ on the permeate flux. It was observed a gradual decrease of the flux during the MD process, until the feed concentration reached the supersaturation point. At that point, the flux decreased sharply to zero. Afterwards, the membrane was completely covered by crystal deposits.

ii. Biological fouling

Biological fouling refers to the attachment to the membrane surface of biological microorganisms such as bacteria, algae and fungi and macro-organisms including mussels, barnacles and hydroids. This type of fouling is significantly affected by MD operation conditions and could be reduced by boiling the wastewater for about 30 min followed by suitable filtration previous to MD [8].

iii. Particulate and corrosion fouling

Particulate fouling may generally be defined as the deposition of solid particles in suspension into the membrane surface. The size of the suspended particles will have very high influence on the deposition rate and mechanism responsible for its transport to the membrane surface [8].

Currently, pretreatment and membrane cleaning are the main techniques to control fouling. Alklaibi et al. [50] investigated the influence of fouling by preparing three different solutions: water pre-treated by microfiltration, seawater and 3% NaCl solutions. They claimed that the pre-treatment process increased the product flux by 25%.

2.1.7. Operating parameters

This section describes the effect of the most significant operating variables on the performance of DCMD systems.

i. Feed temperature

The effect of feed temperature on permeate flux has been widely investigated. It is generally agreed upon that in all MD configurations there is an exponential increase of MD flux with the increase of feed temperature. This is due to the exponential increase of vapor pressure of feed solution with temperature, which increases the transmembrane vapor pressure (i.e. the driving force). Even though temperature polarization effect increases with the feed temperature, it has been proved that working under high feed temperature results in high internal evaporation efficiency (ratio of heat that contributes to evaporation and the total heat exchanged from the feed to the permeate side) [20], [51]–[54].

ii. Feed inlet concentration

MD is a suitable technology for treating highly concentrated solutions that cannot be treated in pressure-driven membrane processes (e.g. RO) due to the extremely high energy requirements [19], [55], [56]. Presence of salts in feed solution results in a reduction of the permeate flux in all MD configurations. This detrimental effect is attributed to the decrease in partial vapor pressure and thus the driving force of MD process [57]–[60]. Alklaibi et al. [61] reported 12% reduction in permeate flux when NaCl concentration increased from 0 to 2M.

iii. Feed circulation velocity and stirring rate

Increasing both feed circulation velocity and feed stirring rate results in a decrease of the boundary layer thickness and thus an enhancement of the heat transfer coefficient at the feed side and a reduction of polarization effects [8]. This reduction of polarization effect implies that temperature at the membrane surface becomes closer to the bulk feed temperature and therefore the transmembrane temperature difference is higher, thus resulting in higher MD permeate flux. The feed flow rate must be varied with due precautions to avoid membrane pore wetting [8].

iv. Permeate temperature

Increasing permeate temperature results in a decrease of the transmembrane vapor pressure, which in turn results in a decrease of permeate flux [8].

v. Temperature difference and mean temperature effect

At constant temperature difference across the membrane, permeate flux exponentially increases with the mean temperature [52], [62].

vi. Permeate flow velocity

An increase of permeate flow velocity increases heat transfer in the permeate side of the membrane module by reducing the temperature polarization effect. This is caused by an enhancement of the heat transfer coefficient in the permeate side, and results in higher permeate fluxes [8].

2.1.8. MD commercial prototypes

Numerous commercially oriented MD technologies have emerged in the last few years. This section focuses on current arrangements of these commercially available MD systems. Today, the most notable organizations specializing in MD technology are:

- Fraunhofer ISE (AGMD)
- Memstill and Aquastill (AGMD)
- Scarab (AGMD)
- Memsys (vacuum enhanced multi effect AGMD)

It is worth noting that all four organizations focus on AGMD systems. This is in agreement with the fact that DCMD systems are mainly used at laboratory scale whereas commercial prototypes are usually build as AGMD due to their higher energy efficiency (see section 2.1.2).

i. Fraunhofer ISE

Fraunhofer Institute for Solar Energy System (ISE) developed a spiral wound AGMD system. These units are built so that membrane areas between 5 and 14 m² can be achieved for a single unit. Thermal energy requirements can be as low as 130 kWh/m³ as reported in [18], representing a Gain Output Ratio (GOR¹) of 4.8.

The section and a picture of the module are presented in Figure 6 (a) and (b), where (1) is the condenser inlet, (2) the condenser outlet, (3) the evaporator inlet, (4) the evaporator outlet, (5) the distillate outlet, (6) the condenser channel, (8) the condenser foil, (9) the distillate channel, and (10) the hydrophobic membrane.

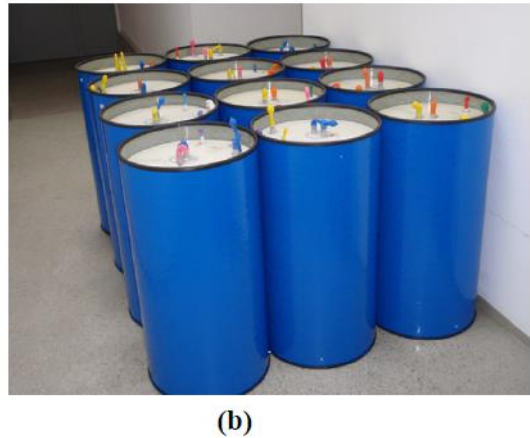
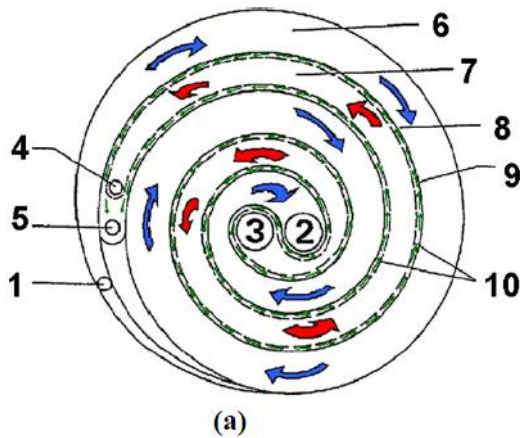


Figure 6. (a) Section of Fraunhofer ISE's spiral wound AGMD module; (b) Picture of the modules [18]

¹ GOR is the latent heat of evaporation per unit mass of product divided by the amount of energy required by the system per unit mass of product.

ii. Memstill and Aquastill

Memstill was developed by the TNO (Netherlands Organisation for Applied Scientific Research) in 2006. This technology (Figure 7) is based on the AGMD concept and has been largely trialed using raw seawater in Singapore, the Netherlands (E.ON Benelux Power Plant), and Port of Antwerp (BASF) [1]. A less successful trial was conducted on brackish water from the harbor of Rotterdam, failing due to lack of monitoring and incorrect pre-treatment [63]. Trialing has featured modules containing up to 300 m² of membrane area. Current plants operate at 100 m³/day scale on a petroleum refinery in Singapore [1]. The thermal energy required, claimed by Memstill in its years of trials, is as low as 56 to 100 kWh/m³ (GOR up to 11.2). This is the lowest value (or higher GOR) reported from real testing. The electrical energy required was assumed to be 0.75 kWh/m³ [64].

The Memstill technology has been licensed to Aquastill and Keppel Seghers for industrial module production. In June 2012, Aquastill's website indicated the availability of both AGMD and DCMD modules.

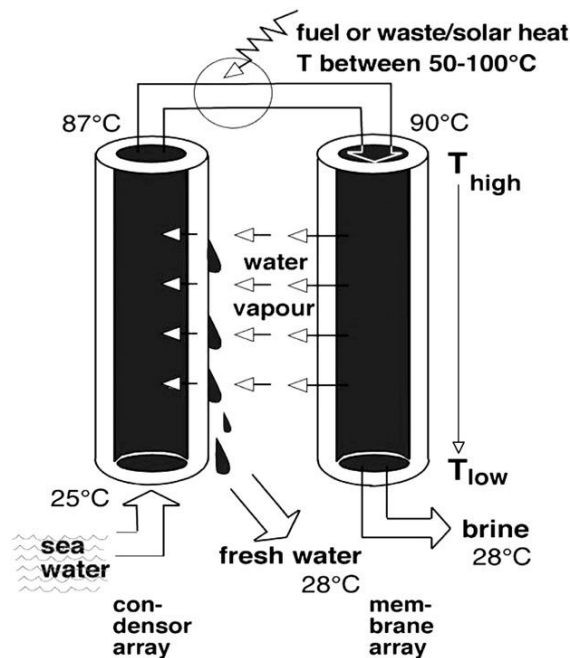


Figure 7. Concept of the Memstill process based around AGMD [64]

iii. Scarab AB

The Scarab AB (Figure 8) system features an AGMD module, and has been trialed in solar ponds in 2004 by University of Texas, and using solar thermal collectors in Spain and Mexico by the MEDESOL project starting in 2008 [65]. In a trial under the MEDESOL project lasting 4 months, issues related to membrane wetting over the longer term were reported. During the trials, fluxes up to $6.5 \text{ kg m}^2 \text{ h}^{-1}$, and thermal consumption of 810 kWh/m^3 (GOR of 0.78) were obtained [66].

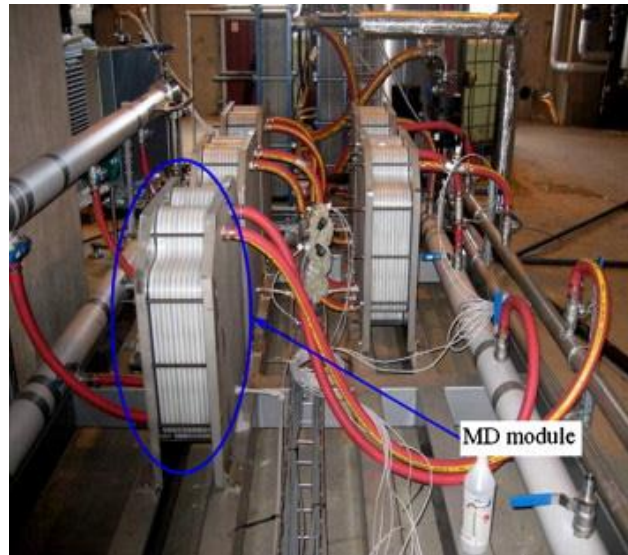


Figure 8.Scarab AB modules [67]

iv. Memsys

The Memsys system is a relatively new MD technology that features a novel internal heat recycling concept that allows for reduced thermal consumption. The heat recycling system, known as Vacuum-Multi-Effect-Membrane-Distillation (V-MEMD) utilizes a multistage setup integrated into a compact plate and frame module. Memsys modules are 330 mm x 700 mm x 480 mm in dimensions, with 3.5 m² of both MD and condensation membranes. The MD membrane is made from PTFE and the condensation membrane is made from metal coated PP [1].

Since module production started in 2010, technical articles with trials are currently unavailable. However, Memsys promises thermal energy requirements of 175-350 kWh/m³ (GOR up to 3.6) and electrical energy requirement of 0.75-1.75 kWh/m³. Memsys technology require feed temperature from 60 to 100°C and cooling <40°C. Fluxes of Memsys systems have been demonstrated in the range of 6.8 to 9.5 kg m⁻² h⁻¹. Current module capacity is specified at 50 m³/day [68].

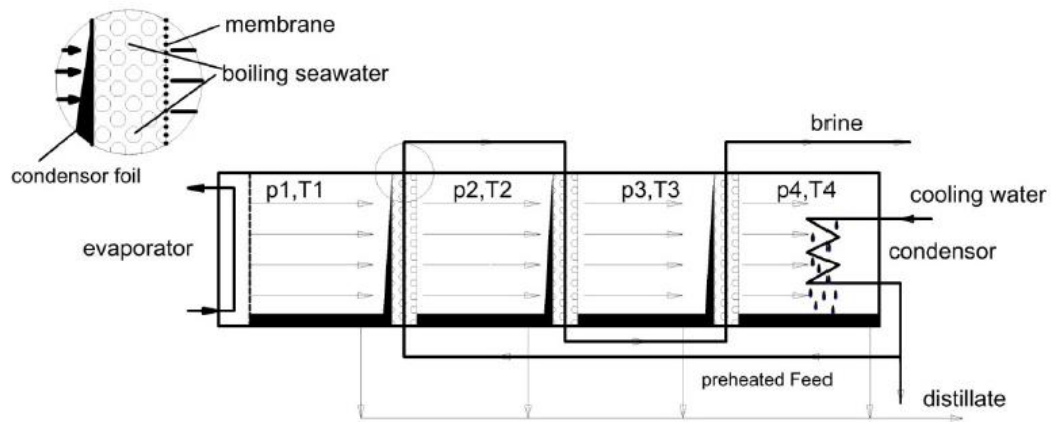


Figure 9. Vacuum-Multi-Effect-Membrane-Distillation (V-MEMD) process from Memsys [68]

Besides developing highly efficient MD systems, efforts are being made in promoting systems combining different technologies to provide ZLD solutions. One of the most significant cases is the MD crystallization. This approach (Figure 10) has been proposed as a solution to remove precipitating salts and hence maximize MD concentration factors² [49], [69], [70]. MD crystallizers have been tested for NaCl and Na₂SO₄ solutions having salinity above saturation [49], [70] and for sea water desalination [69]. It has been found that at certain feed concentrations, sudden flux decline occurred. This was due to crystal formation at the membrane surface, which in turn had detrimental effects to the membrane as salts can penetrate into the pores compromising salt rejection. Further development should focus on favoring salts precipitation in the crystallizer instead of in the membrane.

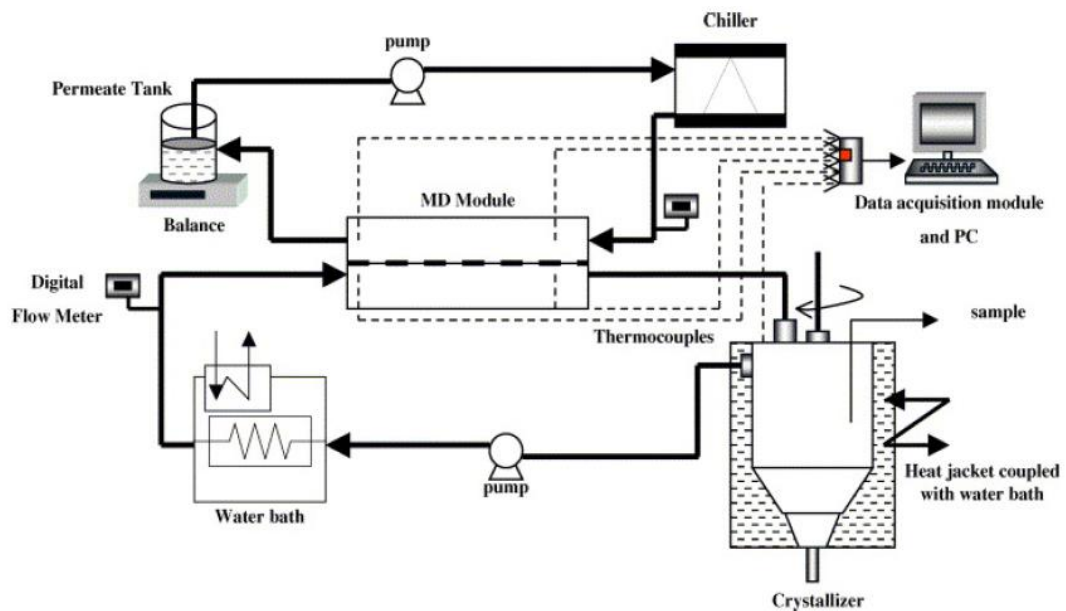


Figure 10. Experimental setup of the MD crystallization used by Tun et al. [49]

² The concentration factor is a parameter used to determine in which degree a solution has been concentrated. It can be calculated as final concentration divided by initial concentration of the solution.

2.2. Aeration and acidification

As it has been mentioned in section 2.1.6, crystallization fouling represents one of the major challenges in brine concentration processes. In order to overcome this problem, a number of brine pretreatment processes have been developed. These processes can be mainly divided in those that focus on removing scaling components prior to MD by causing them to precipitate, and those in which the equilibrium of scaling components is modified so that precipitation is delayed. The former rely on pH changes of feed through the dosage of alkaline reagents such as sodium hydroxide, lime or magnesia to cause components to precipitate. On the other hand, the later techniques rely on the addition of antiscaling products [71].

In this section, aeration and acidification are presented as potential brine pretreatment techniques. Aeration may be included in the category of pretreatments that rely on elimination of scaling components whereas acidification relies only on delaying precipitation.

Stripping of carbon dioxide has been suggested as a chemicals-free technique able to effectively remove carbonates from brine, hence reducing its scaling potential. By applying this technique, the content of carbon decreases due to CO_2 transfer to atmosphere, thus reducing the scaling potential of brine. Besides, under certain pH conditions, CO_2 transfer may cause scaling components to precipitate due to a raise in the pH of brine [71]. Therefore, this technique, also known as aeration, is especially effective in the elimination of carbonates, even though it is able to remove significant amounts of sulfates as well when precipitation occurs.

Since CO_2 stripping is highly affected by solution pH, aeration is usually carried out in combination with acidification in order to achieve maximum CO_2 removal. Acidification is carried out by adding concentrated HCl. If other acids such as H_2CO_3 or H_2SO_4 are used instead of HCl, the concentration of potential scaling components such as CO_3^{2-} or SO_4^{2-} increases, causing a detrimental effect on the pretreatment efficiency.

Acidification can also be applied as a pretreatment technique by itself. By acidifying, the equilibrium of the carbonate system is modified, drastically reducing the presence of CO_3^{2-} . When the concentration of CO_3^{2-} is reduced, the precipitation of CaCO_3 in the MD stage can be significantly delayed. However, unlike aeration, acidification only affects the precipitation of carbonate components.

2.2.1. Theoretical principle

Dissolved CO_2 that is transported in aeration process is part of an aqueous chemical system known as the carbonate system. This system is greatly affected by the pH level of the solution, and in simple aqueous solutions is composed of the following components: carbon dioxide (CO_2), carbonic acid (H_2CO_3), bicarbonate (HCO_3^-) and carbonate (CO_3^{2-}). The equilibrium between these components is given by the following reactions [72]:



Where $H_2CO_3^* = (CO_2 + H_2CO_3)$, and K_1 and K_2 are the first and second dissociation constants of carbonic acid, and can be expressed as described as follows.

$$K_1 = \frac{[H^+][HCO_3^-]}{[H_2CO_3^*]} \quad (25)$$

$$K_2 = \frac{[H^+][CO_3^{2-}]}{[HCO_3^-]} \quad (26)$$

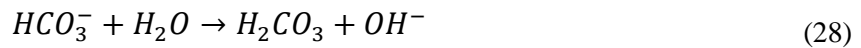
The equilibrium constant for the CO_2 hydration reaction is as low as $K_0 \approx 7 \cdot 10^{-7}$. From this value it follows that the reaction lies rather to the left and therefore the concentration of CO_2 greatly exceeds that of H_2CO_3 [73], [74].

Removing CO_2 from the system will induce an increase in the pH according to the following mechanisms [75]:

- At low pH as CO_2 is removed from the system, new CO_2 will be formed mainly by the dissociation of HCO_3^- to CO_2 to maintain the equilibrium.



- At high pH since the concentration of H^+ is low, CO_2 is formed from HCO_3^- through the reaction with water.



The relation between pH, concentration of CO_2 (aq), CO_3^{2-} and total carbon can be observed in Figure 11. In this figure it can be noticed that pH rises as CO_2 is desorbed. Besides, concentration of CO_3^{2-} increases due to higher pH and TC slowly decreases due to CO_2 desorption.

As it can be seen in the carbonic dissociation diagram in Figure 12, under acidic conditions the carbonate system favors the presence of H_2CO_3 which in turn means that the concentration of $CO_2(aq)$ will be higher. According to Henry's law, the higher the concentration of $CO_2(aq)$, the higher will be the transport of CO_2 to the gas phase.

$$H_{CO_2} = \frac{C_{CO_2(aq)}}{P_{CO_2}} \quad (30)$$

where H_{CO_2} is Henry's coefficient of CO_2 in pure water, and P_{CO_2} the partial pressure of carbon dioxide above the aqueous phase.

The mechanisms behind the effect of acidification following aeration or as a pretreatment itself lies uniquely on the acid carbonic dissociation system. In this case CO_2 stripping does not take place. However, as the pH is displaced to acidic values, the concentration of CO_3^{2-} decreases, i.e. $CaCO_3$ and $MgCO_3$ cannot precipitate.

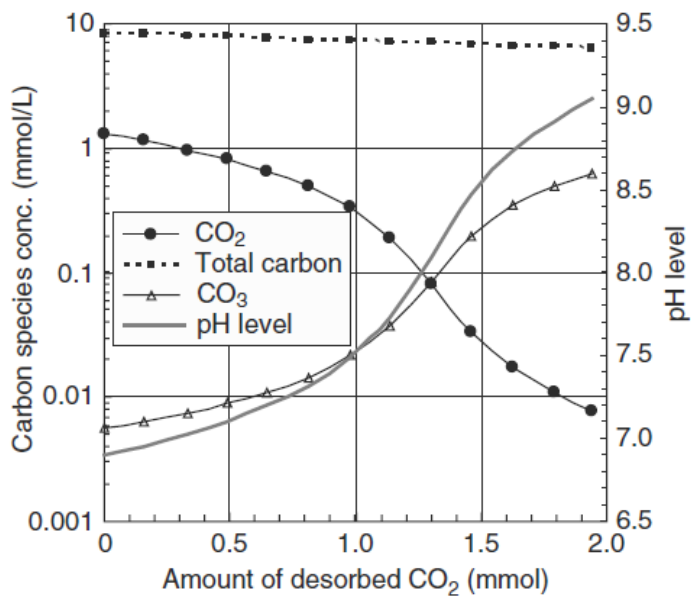


Figure 11. Effect of CO₂ desorption on the pH and on the carbon components distribution [71]

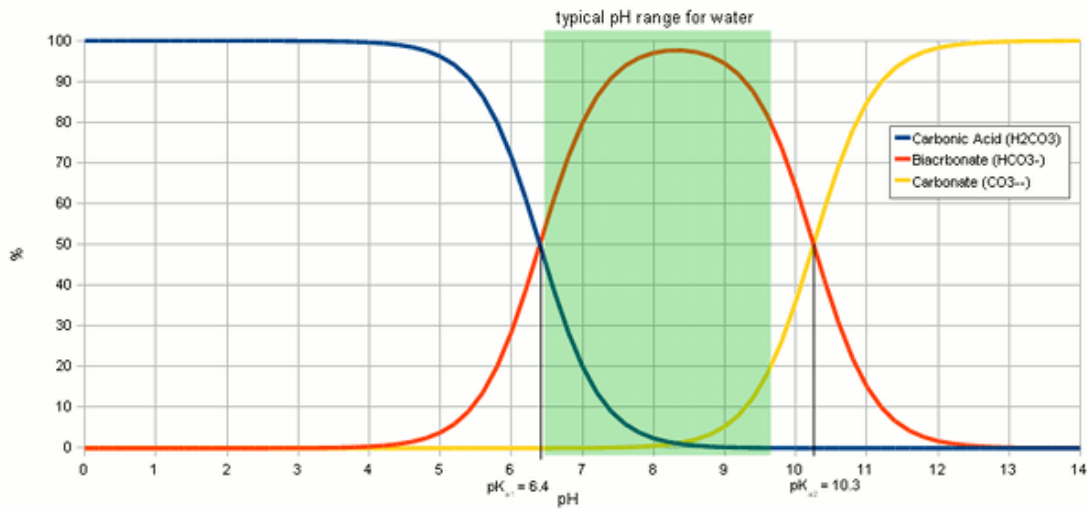


Figure 12. Carbonic acid dissociation [76]

2.2.2. Mass transfer in aeration

Since a change in pH alters the distribution of carbon components, the specific rate of CO₂ desorption (R_{CO_2}), is given by the change in total carbon content (C_T) and not by the change in the CO₂ concentration [71].

$$R_{CO_2} = \frac{N_{CO_2}}{V_L} = -\frac{dC_T}{dt} \quad (31)$$

where N_{CO_2} is the CO₂ desorption time [mol/s] and V_L is the total solution volume.

The kinetics of CO₂ desorption can be characterized by the overall mass transfer equation based on the liquid phase driving force as shown in the following equation [71].

$$R_{CO_2} = -\frac{dC_T}{dt} = K_L \cdot a \cdot ([CO_2]_{bulk} - [CO_2]^{eq}) \quad (32)$$

where K_L is the overall mass transfer coefficient [m/s], a is the interfacial area of the air bubbles per unit solution volume [m^{-1}], $[CO_2]_{bulk}$ is the bulk CO₂ concentration and $[CO_2]^{eq}$ is the concentration of CO₂ at equilibrium with the gaseous phase.

Since evaluation of the interfacial area of the bubbles is difficult, it is customary to define the mass transfer in the system by the magnitude of an overall volumetric mass transfer coefficient $K = K_L \cdot a$ [s^{-1}] which combines the intrinsic mass transfer coefficient with the interphase mass transfer area. This value is determined by representing the plots $-dC_T/dt$ vs. dissolved CO₂ concentration. The slope of the linear curve obtained provides the value of volumetric mass transfer coefficient K as shown in Figure 13; **Error! No se encuentra el origen de la referencia.** [71].

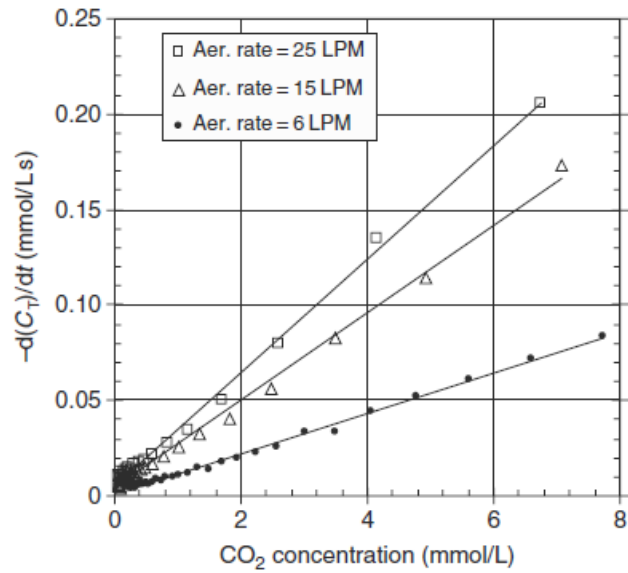


Figure 13. Rate of CO₂ desorption vs. momentary CO₂ concentration [71]

Effectiveness of CO₂ stripping in a given aeration apparatus can be assessed from the magnitude of K achieved in the system. Major parameters affecting the magnitude of K are air flow rate and solution agitation speed [71].

Several contactor types can be used for the physical absorption or desorption of CO₂ in aqueous solution. However, design of such units is still very difficult without the employment of empirical knowledge and experience as well as the use of an extensive amount of pilot-scale testing [72]. This is mainly caused by the very complex hydrodynamic conditions prevalent in these contactors [77]. Agreement exists on the role of the energy input, gas flow rate, liquid flow rate, and temperature (only for the case of desorption) on their positive effect on the value of $K_L a$ [72]. A list of the K_L and $K_L a$ values for different contactor types is presented in Table 3.

Table 3. Characteristics of Gas-Liquid Contacting Equipment [72]

Device	$K_L (\times 10^4 \text{ m s}^{-1})$	$K_L a (\times 10^2 \text{ s}^{-1})$
Packed-column and trickle-bed reactors	0.3 – 2	0.06 – 7
Bubble columns	1 – 4	0.25 – 40
Plate columns	1 – 4	1 – 8
Packed bubble column	1 – 4	1 – 12
Mechanically agitated contactors	1 – 5	
Static mixers	1 – 20	2 – 50
Membrane contactors		10 – 200
Shell-side water flow	0.02 – 1	7.5 – 3.6
Tube-side water flow	0.037 – 1.5	

EXPERIMENTAL PART

3. Materials and methods

This chapter describes the experimental apparatus and procedure, characteristics of the brine used as feed, experimental plan, and applied analysis techniques.

3.1. Experimental equipment

Two experimental modules were used in the experimental study: the MD apparatus and the aeration column.

i. MD apparatus

MD experiments were conducted in a setup consisting of a MD module, a heating bath for the feed, a cooling bath for permeate, a scale connected to a laptop to measure the distillation rate, and two peristaltic pumps. Figure 14 shows the diagram of the MD apparatus.

The MD module was of the type plate and frame, and therefore it worked with a flat sheet membrane. The module was made out of Teflon, having an effective membrane area of 90 cm². The module was handmade and consisted of two identical pieces between which the membrane was placed. In order to monitor heat exchange in the module, one mercury thermometer was installed at each of the four entrances of the module.

In the feed side of the apparatus, heating was provided by a heated bath (Selecta). The feed container was placed inside the heated bath. Since heat transfer between water in the heated bath and the solution in the container was poor, a heat exchanger was installed. The heat exchanger was a glass coil in which the solution from the feed side leaving the module was heated up before going back to the container. The container had a maximum volume of 930 mL.

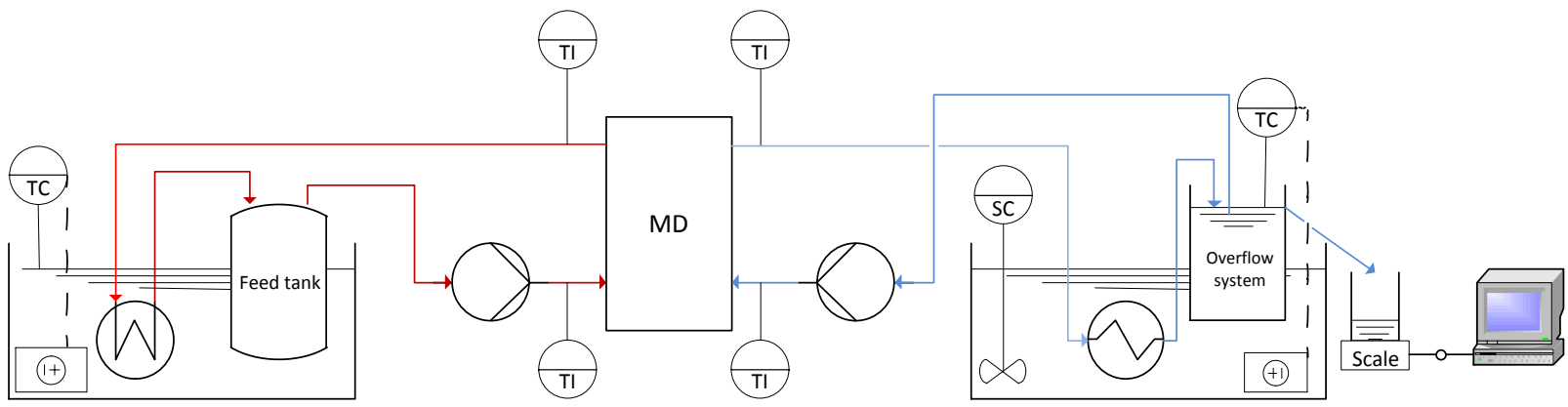


Figure 14. Diagram of the MD apparatus

The permeate side consisted of a cooling bath, an impeller, a heat exchanger, and the overflow system from which permeate exited the loop. The cooling bath was cooled up with an immersion cooler (Selecta). The impeller (Heidolph RZR1) was placed in the bath to enhance heat transfer between the immersion cooler and water in the cold bath. Similarly to the installation in the feed side of the apparatus, a heat exchanger was installed in order to achieve an adequate cooling of permeate exiting the module before it was pumped back. In this case, the heat exchanger consisted of a coil made out of copper. The overflow system was built using a Büchner flask.

A scale (Mettler Toledo PG503-S) was installed to continuously register permeate pouring out of the overflow. Data was automatically logged to a laptop. The peristaltic pumps were manufactured by Cole-Parmer instrument CO. (6-600 rpm).

ii. Aeration column

Aeration experiments were performed in a PMMA column designed and built in the department. The column had a height of 150 cm and an inner diameter of 10 cm, having a total volume of 11.8 L. At the bottom of the column there were two holes; one for sampling and the other one for air supply. A fish tank diffuser was installed at the bottom of the column and connected to the compressor (Herkules Green Silent 150/8/10, service pressure of 10 bar) through a hole in the bottom of the column. Air flowrate was measured with a rotameter. A diagram of the aeration column is presented in Figure 15.

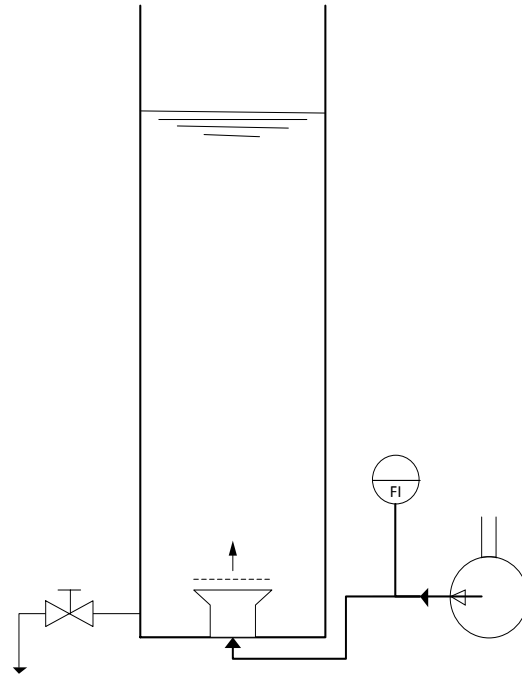


Figure 15. Diagram of aeration column

3.2. Experimental procedure

This section presents the experimental procedure followed in MD and pretreatment experiments.

i. MD experiments

MD experiments were carried out batchwise in the MD apparatus described in the previous section. The container filled with brine was placed in the heated bath, which was adjusted to 65°C and left to heat up for 1h. Analogously, the Büchner flask in the cooling bath (overflow system) was filled up with distilled water and the bath was adjusted to a temperature of 20°C. The impeller was switched on and adjusted at maximum agitation speed. An empty beaker was placed on top of the scale to gather the permeate pouring out of the overflow.

When the mentioned preparative steps had been carried out and the brine had had time to heat up, peristaltic pumps from both circuits were switched on, allowing the brine and the distilled water to fill up the feed and the permeate circuit respectively. Then flowrate of both pumps was adjusted to 0.55 L/min. Finally, the Büchner flask was filled up again until water started pouring out to the empty beaker. When the last drop fell on the container, the scale was adjusted to zero and started to register the weight of distilled water. That was considered the starting point ($t = 0$).

During operation, samples of 5 mL were regularly taken from the feed side to monitor the evolution of dissolved salts. The experiments were stopped when all the brine from the feed side had been distilled. After each experiment the membrane was replaced and the circuit cleaned first with distilled water and then with 0.01M H_2SO_4 in order to remove the scaling that might have had appeared during operation.

ii. Aeration

In aeration runs, 10 L of brine were bubbled for 40 min at an air flowrate of 2 Nm³/h. Samples were regularly extracted from the bottom of the column. When the runs were over, treated brine was collected and the remaining suspended solids filtered out twice. The column was cleaned with distilled water and 0.01M H_2SO_4 .

iii. Acidification

Acidification was carried out using 1M HCl and a pH-meter to control the pH. The beaker in which the acidification was taking place was under agitation.

3.3. Materials

Materials used in experimental tests were brine and hydrophobic membrane. Brine used in all the experiments was collected from the RO unit in the DWTP of Sant Joan Despí. Composition of brine is detailed in Table 4.

Table 4. Raw RO brine composition

Analyte	Concentration (ppm)
Na ⁺	985
Mg ²⁺	282
Ca ²⁺	574
SO ₄ ²⁻	1664
Cl ⁻	1536
TIC	397
TOC	9

where TIC is Total Inorganic Carbon (CO₂, H₂CO₃, HCO₃⁻, CO₃²⁻) and TOC, Total Organic Carbon. In order to be able to achieve the maximum concentration factor in the RO unit, an antiscaling agent is dosed to the water that is being treated before the RO stage. This antiscaling agent remains in the concentrate and hence it is present in RO brine.

On the other hand, the membrane was a PVDF flat sheet membrane. The characteristics of the membrane are presented in Table 5 .

Table 5. Characteristics of membrane

Material	PVDF
Membrane porosity (ϵ)	0.75
Mean pore size (r) (μm)	0.22
Membrane thickness (δ_m) (μm)	110
Liquid Entry Pressure (LEP) (kPa)	204

3.4. Experimental design

The experimental design was planned so that effectiveness of different pretreatment sequences could be evaluated and compared in the MD module. The complete scheme of the experimental design is presented in Figure 16.

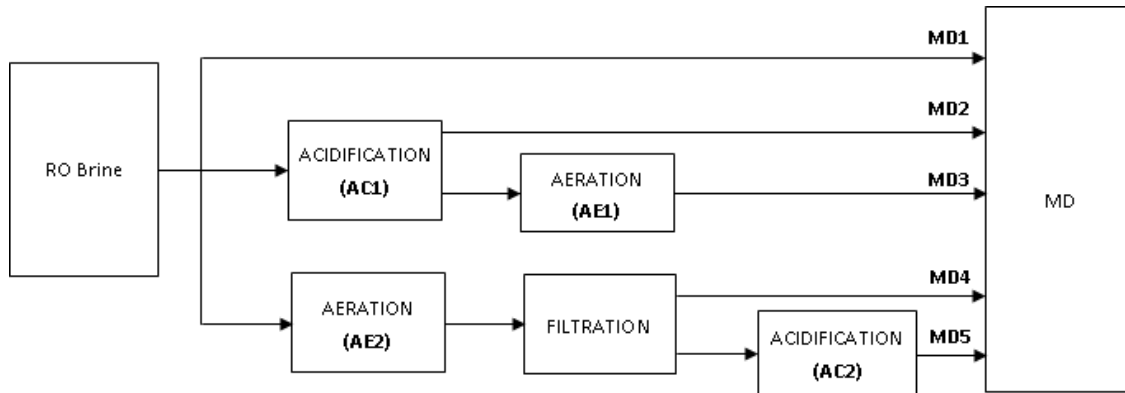


Figure 16. Experimental design scheme

Starting from raw RO brine, five different paths were considered. The first one, MD1, is the straight-out line in Figure 16. In this case no pretreatment is applied to the brine prior to MD in order to have a reference for comparison with the pretreatment sequences. The four sequences left were designed by combining acidification and aeration processes in order to find out which order of application was more effective.

The evaluation of pretreatment was carried out in the MD module (experiments MD1, MD2, MD3, MD4 and MD5). The parameter for evaluation of the pretreatment was the maximum CF achievable without having dissolved salts precipitation. The pretreatment having the higher maximum CF was considered the most effective pretreatment since it provided the major reduction in brine discharge volume.

3.5. Analysis

Three major parameters were monitored in MD runs: Total Inorganic Carbon (TIC), concentration of dissolved salts and pH. In aeration experiments, TIC and pH were monitored; however, concentration of dissolved salts was not monitored due to equipment availability limitations.

i. TIC

TIC was measured in aeration and MD runs so that the total concentration of carbonate components in the water could be monitored. Analyses were performed with Shimadzu TOC-V CPH.

ii. Concentration of dissolved salts

The concentration of dissolved salts was measured using ion chromatography technique in order to be able to determine the maximum concentration factor that could be achieved in the distillation of different pretreated brines. Analyses were performed with a DIONEX ICS 1000 (for cations) and ICS1100 (for anions). In addition to ICS analysis, salts precipitated during MD runs were extracted from the membrane surface and analyzed by SEM/EDS technique. This analysis was carried out in order to confirm that ICS results were correctly performed and analyzed.

iii. pH

Since pretreatment processes studied in this work are greatly affected by pH, a pH-meter (Crison) was utilized to monitor pH variations during both aeration and MD experiments.

4. Results and discussion

4.1. Experimental conditions

This section presents the experimental conditions under which experiments were carried out.

The exact amount of HCl 1M added to bring the pH to a value of 4 is presented in Table 6 in terms of mL of acid per liter of brine.

Table 6. Experimental conditions of acidification

Run	pH _i	pH _f	HCl 1M (mL/L of brine)
AC1	6.9	4.01	26.1
AC2	7.34	4.04	13.6

As it can be observed in Table 6, the amount of acid required for AC2 was significantly lower than the one required for AC1. This is due to the fact that concentration of components from the carbonate system greatly decreased during the aeration stage carried out prior to AC2 (AE2). Since concentration of these components was lower in AC2 than in AC1, there were less HCO_3^- to be neutralized and hence a smaller amount of acid was required to achieve pH 4.

The conditions under which aeration runs AE1 and AE2 were carried out are presented in Table 7.

Table 7. Experimental conditions of aeration

Volume of brine	10 L
Air flowrate	2 Nm ³ /h
Duration	40 min

Finally, the experimental conditions under which the MD runs were carried out are detailed in Table 8.

Table 8. Experimental conditions of MD runs

Run	Temperature (°C)				Flowrate (L/min)		Initial feed volume (mL)
	Feed		Permeate		Feed	Permeate	
	in	out	in	out			
MD1	54	51	21	24	0.55	0.55	500
MD2	54	51	21	24	0.55	0.55	930
MD3	54	51	21	24	0.55	0.55	930
MD4	54	51	21	24	0.55	0.55	930
MD5	54	51	21	24	0.55	0.55	930

Table 8 shows that experimental conditions were the same in all experiments but MD1, in which the initial feed volume was 500 mL instead of 930 mL. This can be explained by the fact that when experiments started, the only suitable container available had a capacity of 500 mL. Since it was desired to increase the amount of initial feed, higher containers were purchased and utilized in the rest of experiments.

4.2. Experimental results

In this section, the results obtained in aeration and MD runs are graphically presented and discussed.

4.2.1. Aeration

Two aeration runs were carried out during this study. In the first one (AE1), acidified brine having an initial pH of 4.3 was used as feed whereas in AE2 the aerated brine was raw. The diagrams corresponding to AE1 and AE2 are presented in Figure 17 and Figure 18 respectively.

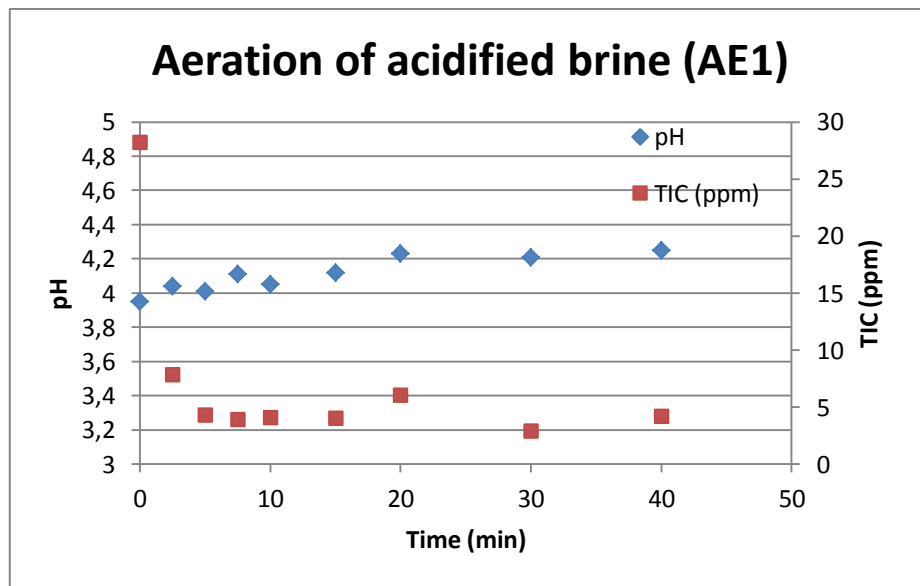


Figure 17. Aeration of acidified brine (AE1)

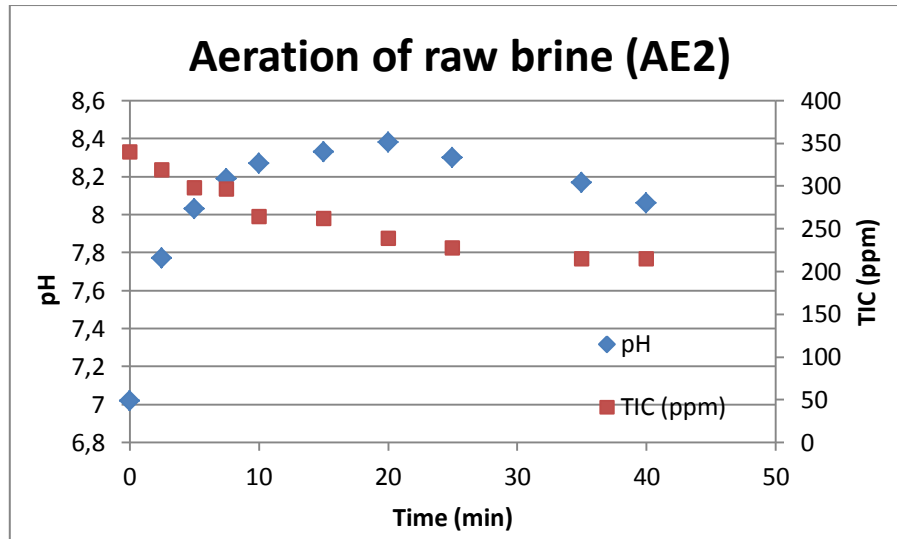


Figure 18. Aeration of raw brine (AE2)

In Figure 17 it can be observed that TIC quickly decreased from around 30 ppm to 4 ppm, where it stabilized. Two remarks can be done by comparing these values to those shown in Figure 18; on one hand it can be observed that only by acidifying the brine and transferring it from the container to the aeration column, TIC is reduced by up to 90%, reaching values much lower than those obtained after aerating raw feed for 40 minutes. On the other hand, it is noticeable that the stabilization time for TIC concentration is much lower in AE1 than in AE2 (4 and 35 minutes respectively). The lower TIC values achieved in AE1 are a direct effect of the acidic pH. At pH values around 4, the carbonate system is displaced toward the acid (H_2CO_3), which in aqueous solution is present as $\text{CO}_2(\text{aq})$. Therefore, having low pH causes the concentration of $\text{CO}_2(\text{aq})$ to increase, enhancing its transfer to the atmosphere.

Both diagrams show that pH values tend to increase as CO_2 is transferred to the atmosphere. This increase is significantly higher in AE2 than in AE1, where the pH rise is lower than 0.5. The higher pH rise in AE2 might be due to a higher concentration of HCO_3^- , which reacts to form CO_2 consuming H^+ (at low pH) or rendering OH^- (at high pH). Since concentration of HCO_3^- in AE1 is much lower than the one in AE2, the consumption of H^+ in AE1 will be much lower than the creation of OH^- in AE2, causing therefore a lesser impact on the pH.

Even though it is not reflected in the diagrams of AE1 and AE2, it is worth knowing that precipitation of dissolved salts could be observed during AE2, whereas salts precipitation did not occur in AE1. This is explained by the fact that under the acidic conditions prevailing in AE1, the concentration of CO_3^{2-} was too low to react with the Ca^{2+} present and precipitate.

4.2.2. MD

MD experiments were analyzed from two different points of view; the first one focuses on the permeate flux achieved in each configuration, whereas the second one focuses on the evaluation of the pretreatments applied.

4.2.2.1. Permeate fluxes

The permeate fluxes obtained for each MD run are presented in Table 9.

Table 9. Permeate fluxes in MD runs

	Permeate flux (mL/min)
MD1	1.43
MD2	1.44
MD3	1.44
MD4	1.43
MD5	1.33

As it can be seen in Table 9, almost all the permeate fluxes obtained were very similar. This was expected since the hydrodynamic conditions were the same for all the runs. The only run that yielded a slightly lower flux was MD5. This might have been caused by a wrong adjustment of the peristaltic pumps that drove the feed and permeate through the module. By expressing the permeate fluxes in terms of $\text{kg/m}^2\cdot\text{h}$, a value of 9.6 is obtained. This value is well in the range of fluxes reported for MD experiments in several papers [12].

Figure 19 presents the distilled water production for experiment MD1. The permeate flux is the slope of the straight line obtained by representing accumulated volume versus time. Even though they appear like an adjusted line, the blue line is just the result of plotting the experimental points.

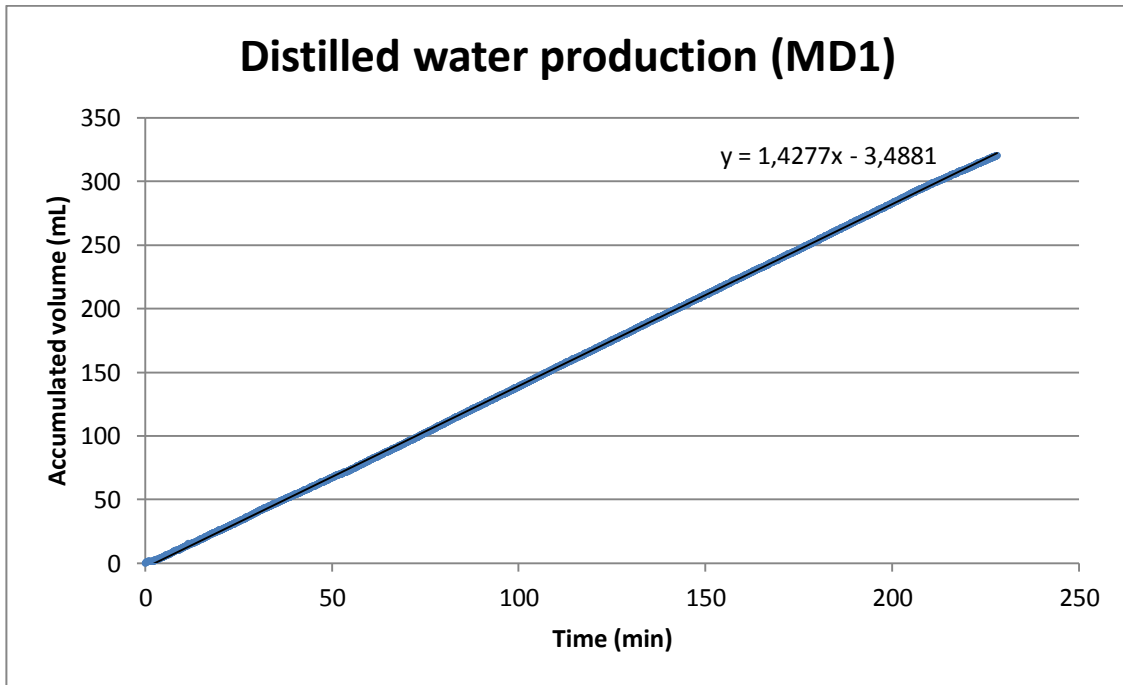


Figure 19. Distilled water production

Since concentration of brine increases as water is distilled, it could be expected to see a gradual decrease of the permeate flux in the diagram due to a lower vapor pressure in feed (see section 2.1.5.2). Eventually it could even be expected to have an even more abrupt decrease of permeate flux due to precipitation of salts onto the membranes. However, as it can be seen in Figure 19, the permeate flux was constant throughout all MD experiments, meaning that neither the higher concentration nor the precipitation of salts affected the process. This can be explained by the low concentration of the brine used in this particular case study, which is typical from an RO system treating water from a river in a water purification plant.

In order to see how severe permeate flux decrease could be, an experiment was carried out in which a NaCl solution was distilled in the MD module instead of brine. The solution had a concentration of 200g/L and was distilled in the exact same conditions as the MD experiments. The results of these experiments are presented in Figure 20.

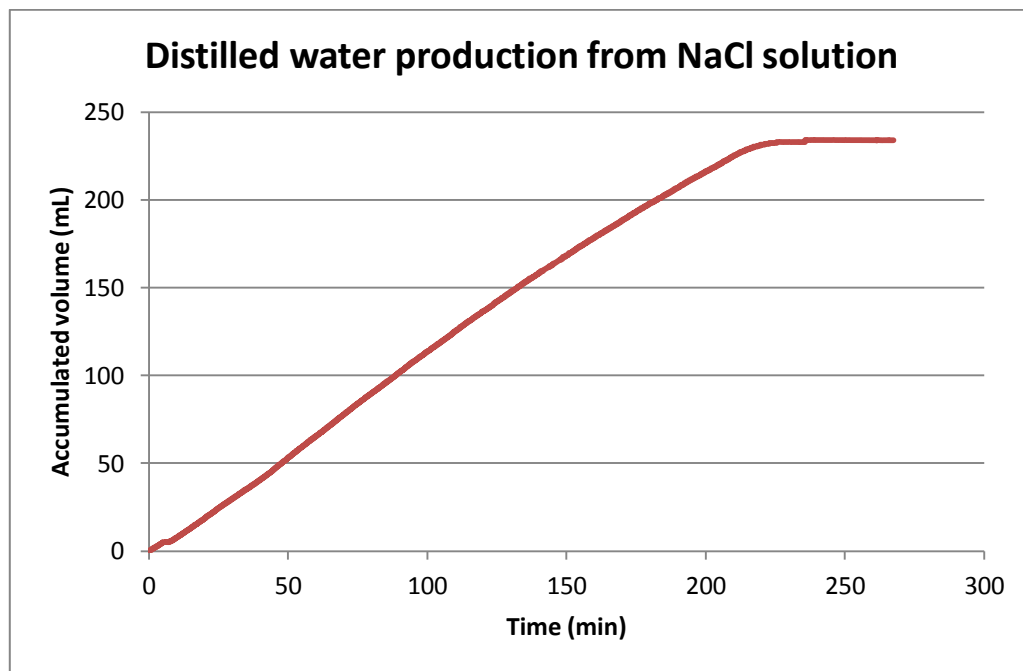


Figure 20. Distilled water production from NaCl solution

Figure 20 shows that when high salt concentrations are achieved the permeate flux decreases and even stops. It is believed that the flux decrease and finally are mainly caused by the precipitation of salts instead of by the higher concentration. However, this has not been proved in this work.

4.2.2.2. Evaluation of pretreatments

In order to evaluate the efficiency of the different pretreatment sequences presented in the previous chapter, a sample of pretreated brine from each was distilled in the MD module, in which concentration of ions was monitored. Results of this monitoring are presented in diagrams from Figure 21 to Figure 25. In these diagrams, CF of each ion in front of the time is represented. This sort of diagram has been selected because it allows for an easy identification of the maximum CF and the precipitating components. If all the components have the same CF it means that they are all being concentrated in the same proportion as feed brine, and hence precipitation has not occurred yet. However, when an ion or ions have a CF lower than the rest, it can be stated that these ions are precipitating. The maximum CF for each experiment is indicated by the blue line.

As mentioned in the previous chapter, a MD run was performed with raw brine in order to set the reference of the maximum CF achievable without applying any pretreatment to brine. The results of this experiment (MD1) are presented in Figure 21.

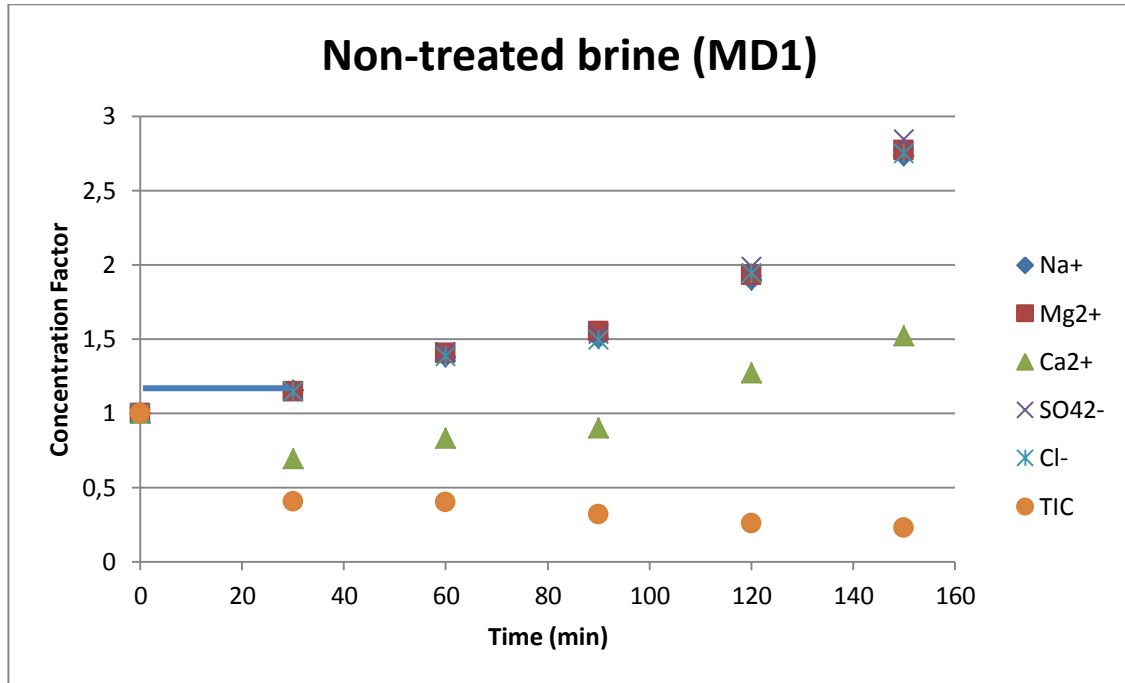


Figure 21. Non-treated brine (MD1)

Figure 21 shows that raw feed is very close to the saturation point. This can be seen by observing the CF of Ca^{2+} , which is lower than the rest from the first analysis ($t = 30$ min). Since SO_4^{2-} has the same CF as the rest of ions, it can be stated that the component being precipitated is CaCO_3 . This could also be interpreted by analyzing the tendency of TIC. However, a decrease in the concentration of TIC can be also caused by CO_2 transfer to the atmosphere. The concentration of TIC in these experiments might lead to misleading conclusions and should be only used to corroborate the conclusions extracted from the CF of the ions.

The diagram corresponding to the run evaluating acidification as a pretreatment (MD2) is presented in Figure 22.

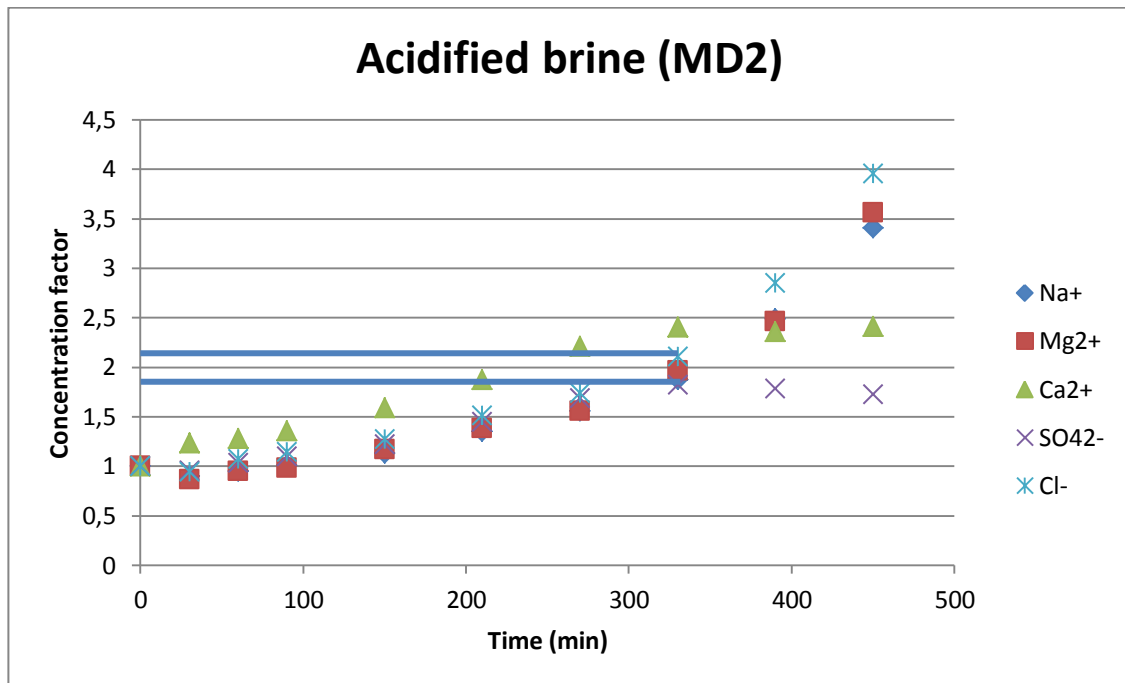


Figure 22. Acidified brine (MD2)

Figure 22 shows that only by acidifying raw brine, the maximum CF before precipitation can be practically doubled. Due to problems with the analyzer, there is not TIC data available for this diagram. Nevertheless, it can be seen that the first component that precipitated was CaSO_4 (the CF of both ions follow the exact same tendency). The fact that CaSO_4 precipitates before CaCO_3 (as happened in MD1) can be attributed to the low amount of CO_3^{2-} caused by the low pH.

It is worth mentioning that even though the starting pH was approximately 4, the final pH was 7.4. The pH rise during MD is believed to be caused by the CO_2 transfer to the atmosphere. This pH rise has a very positive connotation from a commercial point of view as it shows that an acidification pretreatment can be carried out without having an acidic output, which would be costly to dispose of.

The diagram corresponding to the run evaluating acidification followed by aerations as a pretreatment (MD3) is presented in Figure 23.

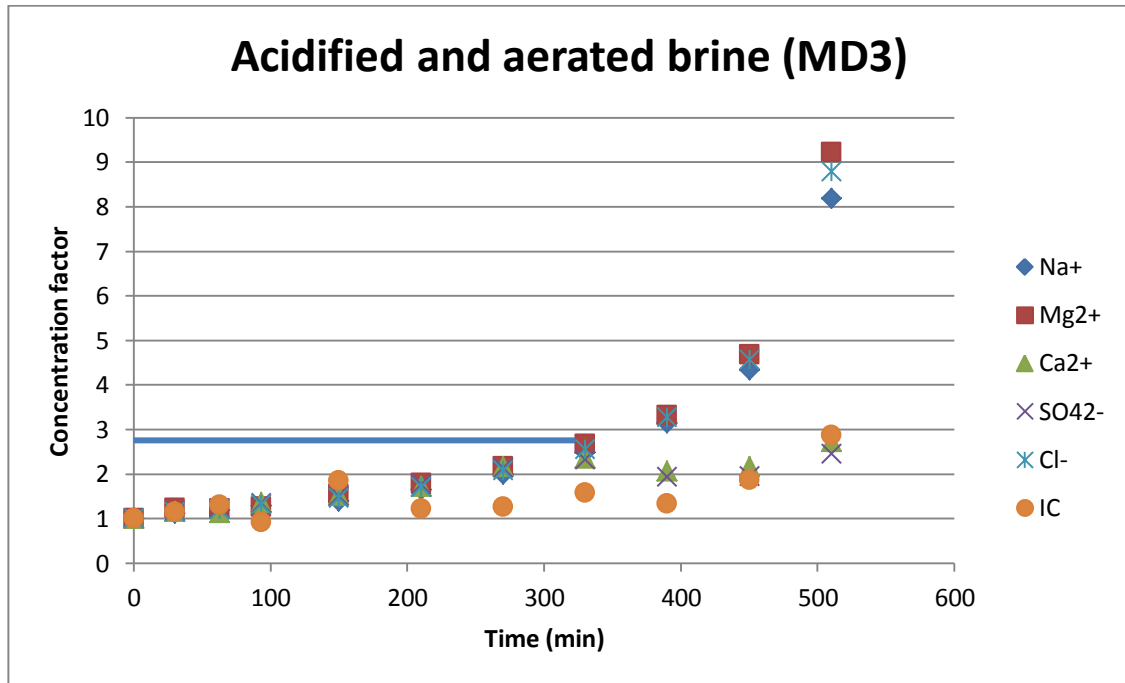


Figure 23. Acidified and aerated brine (MD3)

In Figure 23, a similar trend to the one obtained in Figure 22 can be observed. In this case (MD3), however, the maximum CF achievable is slightly higher than in the previous (MD2). From a theoretical point of view, this difference cannot be attributed to the aeration since the first precipitating component in both cases is CaSO_4 and aeration should only affect the carbonate system. This higher CF could be explained if precipitation of any component containing Ca^{2+} occurred during aeration. However, no precipitating components were observed during aeration at low pH.

Another possible explanation is that the precipitation of CaSO_4 is affected by the concentration of CO_3^{2-} so that a lower concentration of the latter delays the precipitation of the former. However, the relationship between ions was not investigated in this work.

The diagram corresponding to the run evaluating aerations as a pretreatment (MD4) is presented in Figure 24

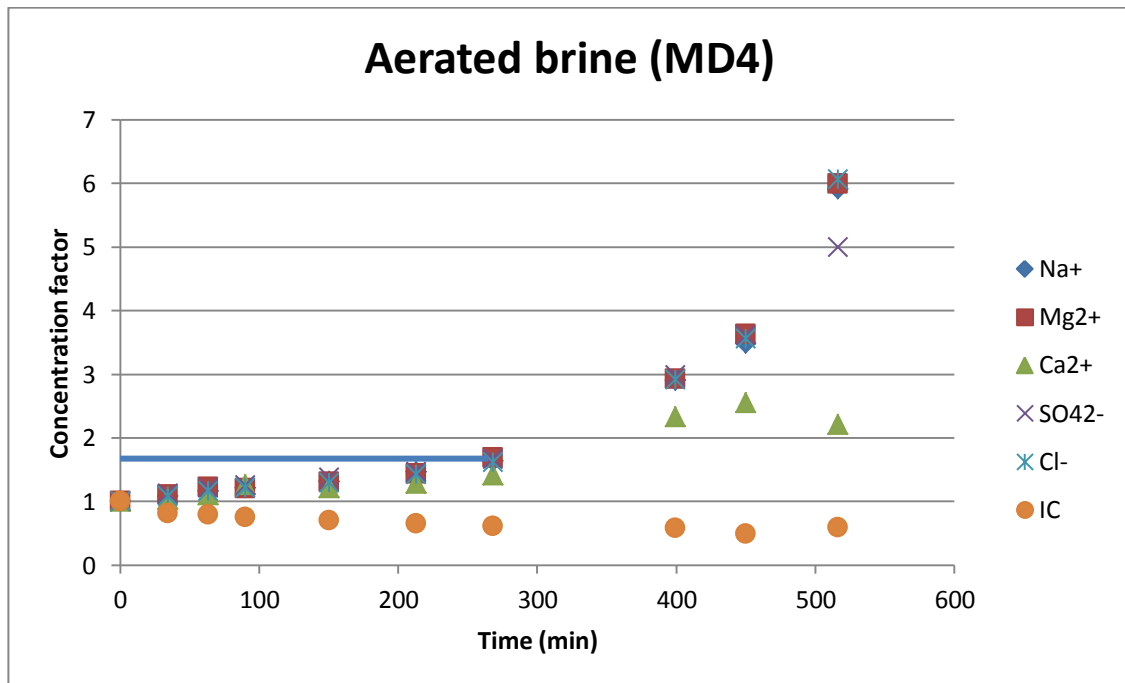


Figure 24. Aerated brine (MD4)

Figure 24 shows that aeration as a unique pretreatment is not very effective. By applying this technique, a CF of 1.6 can be achieved, and the first precipitating component is CaCO_3 . This means that, unlike MD2 and MD3, aeration does not result in significant reduction of carbonates. This is align with Figure 18 (corresponding to AE2), where after 40 minutes of aeration TIC was decreased from 350 to 225 ppm.

The poor performance of this method (MD4) might be caused by an insufficient air flowrate. It is believed that higher air flowrates would enhance the CO_2 transfer to the atmosphere and hence the effectiveness of aerations as a brine pretreatment technique.

Finally, the diagram corresponding to the run evaluating the aeration followed by acidification is presented in Figure 25.

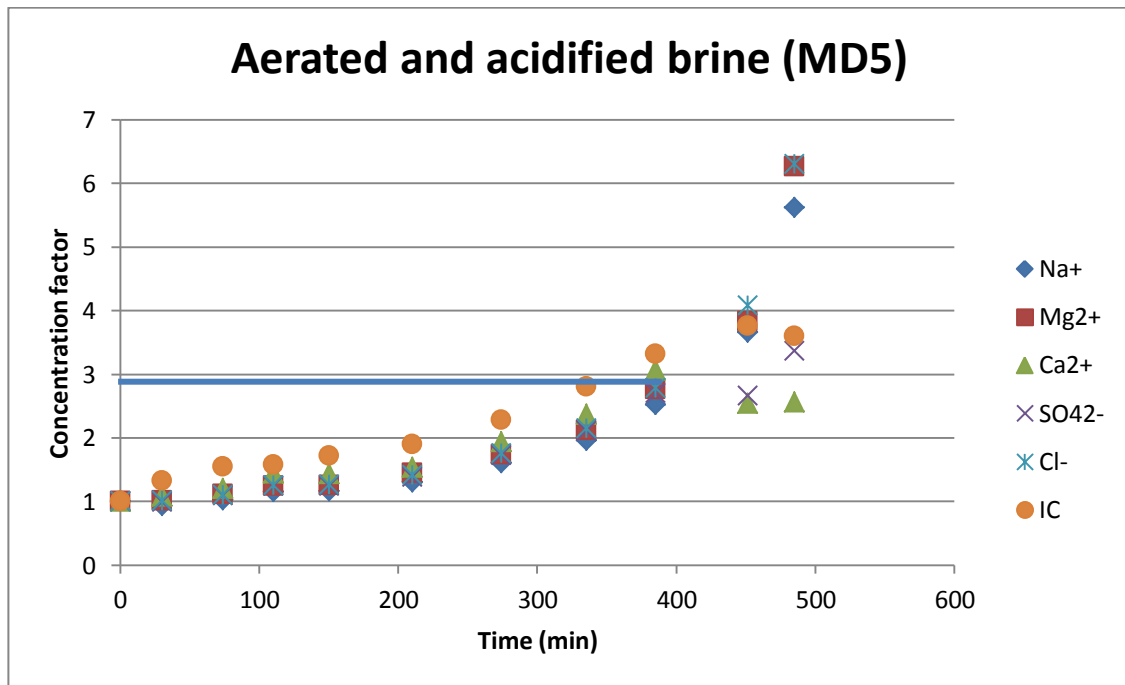


Figure 25. Aerated and acidified brine (MD5)

The highest CF among all the experimental runs carried out in this work was observed in MD5 (Figure 25). The CF obtained in this case is slightly higher than the one obtained in MD3, in which the same pretreatments were applied but in the inverse order. The fact that better results were obtained for MD5 might be due to the precipitation of components containing Ca^{2+} during aeration (AE2). This precipitation, which did not occur in AE1 removed a certain amount of Ca^{2+} . The removal of Ca^{2+} from the system might have caused the delay in the precipitation of CaSO_4 , which was the first precipitating component.

By comparing MD5 with MD4 it can be observed that the maximum CF can be doubled only by adding 13.6 mL of 1M HCl per liter of brine.

In order to verify the analytical results obtained by chromatograph (ICS), precipitated salts from the membrane were analyzed with the SEM/EDS technique. Due to availability limitations of the SEM/EDS equipment, only two samples could be analyzed. One sample was selected in which CaCO_3 was expected (MD4), and the other one in which CaSO_4 was expected (MD3) according to the results obtained from ICS.

The SEM/EDS results for these two cases are presented in Figure 26. Picture (a) and (b) are from the analysis of MD3, while pictures (c) and (d) belong to the analysis of MD4 precipitate.

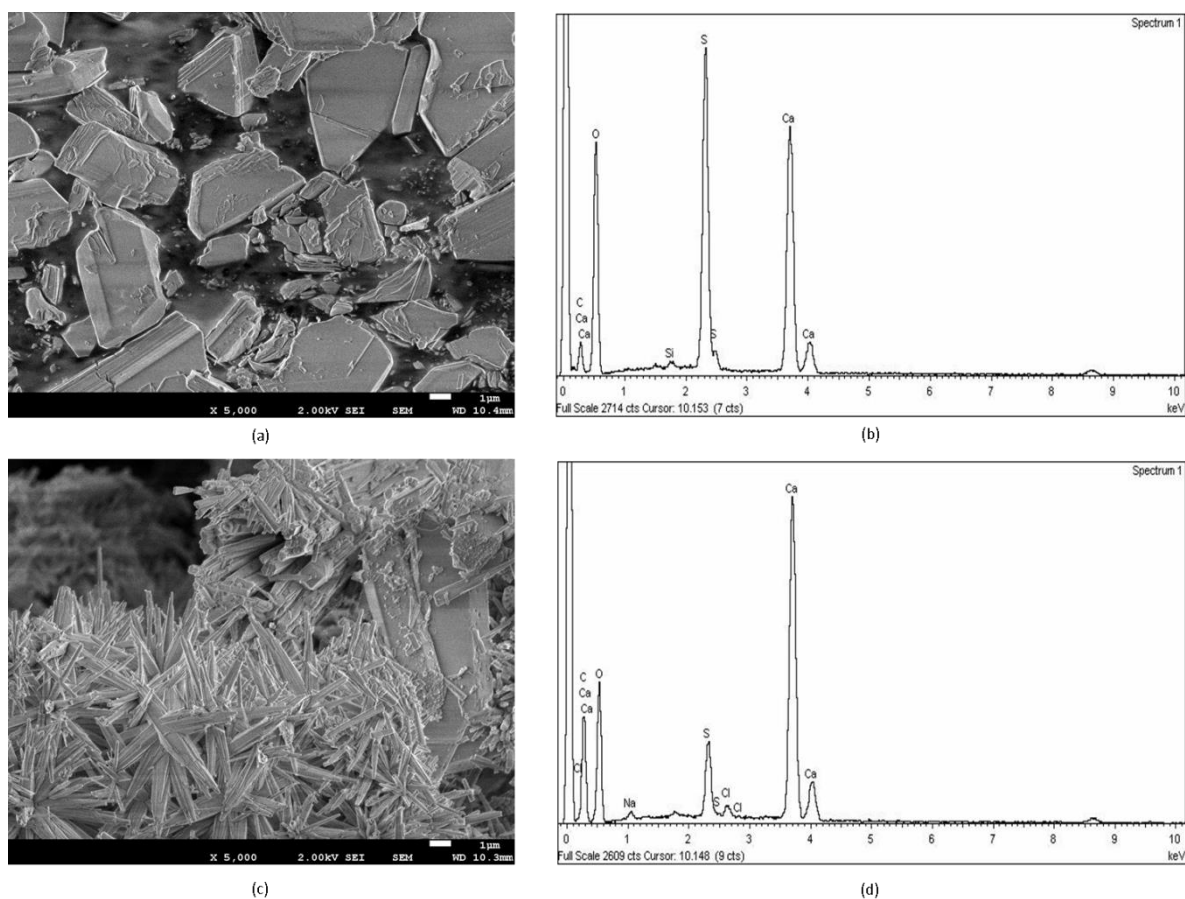


Figure 26. Results of SEM/EDS of MD3 (a, b); and MD4 (c, d)

Figure 26 shows that the crystals obtained for MD3 and MD4 runs (pictures (a) and (c) respectively) are different in shape and in volume. The crystals in picture (a) are flat and wide, while crystals in picture (c) are narrow and pointy. Pictures (b) and (c) show that sulfur concentration is much higher in MD3 than in MD4. Taking into account that CaSO_4 and

CaCO₃ were the two only precipitating components, it can be concluded that the crystals shown in picture (a) are CaSO₄ crystals, and that the ones shown in picture (c) are CaCO₃ crystals.

A summary of the results obtained in the evaluation of the different pretreatments tested is provided in Table 10 and in Figure 27.

Table 10. Summary of the pretreatment evaluation

	MD1	MD2	MD3	MD4	MD5
Pretreatment	-	AC	AC+AE	AE	AE+AC
CF	1.2	1.8 – 2.2	2.75	1.6	2.85
Dominant precipitating component	CaCO ₃	CaSO ₄	CaSO ₄	CaCO ₃	CaSO ₄

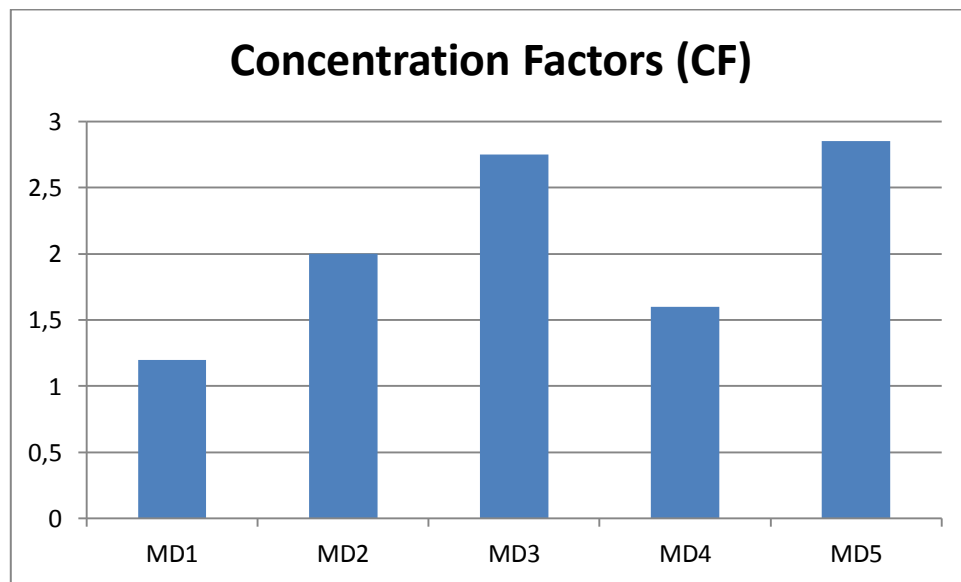


Figure 27. Concentration Factors (CF)

As observed from Table 10 and Figure 27 it can be said that aeration must be improved before it can be applied as a technique by itself. Nevertheless, by applying acidification, the CF can be doubled in a simple and quick manner, which requires no equipment and only consumes HCl.

When higher CF are to be achieved a combination of aeration and acidification is the best option. On one hand, acidifying first, the CF is a bit lower and the acid consumption higher.

Nevertheless, no precipitate is formed and therefore the filtration stage can be omitted. On the other hand, if aeration is carried out prior to acidification, the acid consumption is lower and the performance higher. However, a filtration stage is required to separate those components that precipitate during aeration.

From the results obtained in the MD experiments, it can be also concluded that the components that are most prone to precipitate are Ca^{2+} as cation and CO_3^{2-} followed by SO_4^{2-} as anions. In experiments MD2, MD3 and MD4, SO_4^{2-} was the first anion to precipitate when the concentration of CO_3^{2-} had been lowered. Therefore, by decreasing CO_3^{2-} , the scaling problem is not solved, because SO_4^{2-} can also precipitate as long as the concentration of Ca^{2+} in the solution is high enough. One potential method to decrease Ca^{2+} concentration is aeration, causing CaCO_3 or CaSO_4 to precipitate prior to MD.

To sum up, all those pretreatments sequences that rely only on the decrease in CO_3^{2-} concentration will have a limited performance because SO_4^{2-} will precipitate shortly after in form of CaSO_4 (from our experience the highest CF would be close to 3). If CF higher than 3 are to be achieved, Ca^{2+} removal should be carried out before MD. In this regard, MD5 holds a great potential if higher Ca^{2+} elimination ratios can be achieved in the aeration stage.

5. Economic pre-feasibility analysis

This chapter is devoted to the study of process feasibility from an economic perspective. Since pretreatment technologies proposed for the case study are still in an early development stage, this analysis can only aim to compare in terms of OPEX technologies developed in this work with other ZLD technologies to determine whether or not efforts should be put on further developing aeration and MD. This study does not aim to give an accurate estimation of the economic potential for the technology proposed. The accurate estimation should be left for further studies in which more detailed information from real experience operation is available.

In this analysis, OPEX of different brine disposal options were compared. These options are schematized in Figure 28, and consist in (i) discharge to the medium, (ii) brine crystallization, (iii) acidification followed by MD and crystallization, and finally (iv) acidification and aeration followed by MD and crystallization.

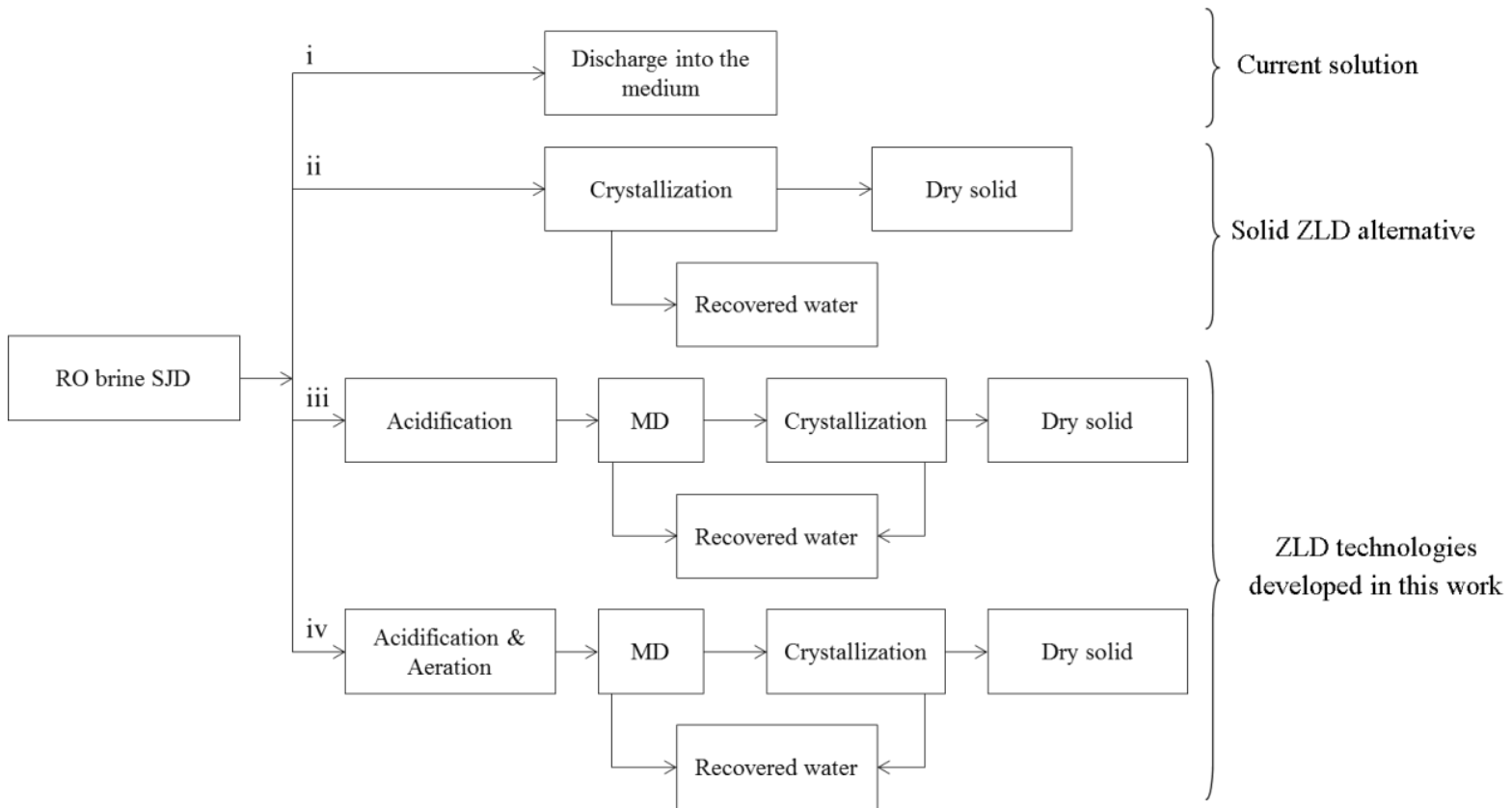


Figure 28. Brine disposal options

Options iii and iv correspond respectively to MD2 and MD3 followed by a crystallization stage, which has been added in the economic analysis even though it was not tested in the experimentation. Since the product of our technology is concentrated brine a further stage is required to achieve ZLD. Crystallization has been selected in this case due to its maturity.

MD2 has been selected for the economic study due to its high performance compared to the ease of operation. On the other hand, MD3 has been preferred rather than MD5 because they both had practically the same efficiency and the latter requires a filtration stage, which is difficult to quantify in terms of OPEX.

For this study, real operation data from Sant Joan Despí DWTP were used. The only information which is common for all options is the brine produced, which is 1584 m³/h. A brief description of the assumptions made for the economic study is presented below for each of the options presented. Following, in Table 11, expenses, revenues and total balance is presented for each option.

i. Discharge into the medium

The first option presented in the scheme is the RO brine disposal solution being currently applied in Sant Joan Despí DWTP, where the generated brine is discharged into a canal which flows into the Mediterranean Sea at a distance of 3.5 km from the coast of Barcelona. Therefore, the only cost derived from the brine disposal derives from its discharge to the medium. This cost can be calculated according to the following equation, which was obtained from the Catalan Water Agency [79]

$$\text{Cost of discharge} = 7.7845 \cdot \text{Conductivity} \quad (33)$$

in which *Cost of discharge* is expressed in €/m³ and *Conductivity* in S·cm⁻¹. The number 7.7845 is a coefficient determined by the Catalan Water Agency.

Knowing that conductivity of SJD RO brine is approximately 0.01 S·cm⁻¹, cost of discharge is:

$$\text{Cost of discharge} = 7.7845 \cdot 0.01 \quad (34)$$

$$\text{Cost of discharge} = \mathbf{0.078 \text{ €/m}^3} \quad (35)$$

ii. Brine crystallization

Option number two was selected so that the process developed in this work could be compared to a solid ZLD competing technology. Cost of crystallization was obtained from reference [80], in which the range 0.6 – 23.9 €/m³ was given for brine crystallization. The average value has been used for this study:

$$\text{Cost of crystallization} = \frac{0.6 + 23.9}{2} \quad (36)$$

$$\text{Cost of crystallization} = \mathbf{12.25\text{€/m}^3} \quad (37)$$

in this case, as well as in case iii and iv, the revenue obtained from recovered water has to be taken into account. According to the Catalan Water Agency [81], the average price of water in Barcelona area is 2.512 €/m³.

The cost derived from disposing of the dry solid is not significant and has not been considered in this analysis

iii. Acidification followed by MD and crystallization (MD2)

In this option, the expenses related to acidification need to be considered. Most of HCl sold in Spain is produced at Bayer facilities in Tarragona. This HCl has a concentration of 30% [82]. Market price of HCl fluctuates according to Bayer selling strategies, however, a value of 100 €/t can be assumed representative within this fluctuations [83]. Acidification cost (€/m³ brine) is calculated as follows:

$$\text{Acidification cost} = \frac{\text{HCl Consumption}}{\text{Market Concentration HCl}} \cdot \text{Market price HCl} \quad (38)$$

where *HCl consumption* is expressed in $\text{mol}_{\text{HCl}}/\text{m}^3 \text{ brine}$, *Market Concentration HCl* in $\text{mol}_{\text{HCl}}/t_{\text{HCl}}$ and *Market price HCl* in $\text{€/}t_{\text{HCl}}$. According to experiments carried out, the amount of HCl 1M required equals 26.1 mL per L of brine ($26.1\text{mol}_{\text{HCl}}/\text{m}^3 \text{ brine}$). The market concentration of HCl is 30% weight ($8228.19 \text{mol}_{\text{HCl}}/t_{\text{HCl}}$). Finally, as indicated in the previous paragraph, market price of HCl is 100 €/t_{HCl}. Knowing this, acidification cost is:

$$\text{Acidification cost} = \frac{26.1}{8228.19} \cdot 100 \quad (39)$$

$$\text{Acidification cost} = \mathbf{0.32 \text{ €/m}^3_{\text{brine}}} \quad (40)$$

The cost of MD was extracted from references [50], [84], [85]. In their studies they claimed OPEX for MD as low as 1.07, 1.21 and 1.19 €/m³. It is assumed that MD works on waste heat and therefore no energy costs are contemplated for brine heating. Average value has been calculated and used for this study.

$$\text{Cost of MD} = \frac{1.07 + 1.21 + 1.19}{3} \quad (41)$$

$$\text{Cost of MD} = \mathbf{1.16 \text{ €/m}^3} \quad (42)$$

The last calculation that needs to be done for option iii is the flowrate of brine that is treated in the crystallizer. This is calculated with experimental CF (2) as shown as follows.

$$\text{Flowrate}_{\text{Cryst}} = \frac{\text{Flowrate}_{\text{MD}}}{\text{CF}} \quad (43)$$

$$\text{Flowrate}_{\text{Cryst}} = \frac{1584}{2} = \mathbf{792 \text{ m}^3/\text{h}} \quad (44)$$

iv. Acidification and aeration followed by MD and crystallization

Most of the inputs of the economic analysis for this option have already been detailed in the previous ones. The only input left is the cost of aeration, which is calculated as detailed in the following equation:

$$\text{Aeration cost} = \text{Compressor power} \cdot \text{Compressor usage} \cdot \text{Electricity price} \quad (45)$$

where *Aeration cost* is expressed in terms of €/m³_{brine}, *Compressor power* in kW, *Compressor usage* in h/m³_{brine} and *Electricity price* in $\frac{\text{€}}{\text{kW}\cdot\text{h}}$

The time that the compressor has to work per cubic meter of brine is calculated as follows:

$$\text{Compressor usage} = \frac{\text{Length of aeration runs}}{\text{Volume treated}} \quad (46)$$

where *Length of aeration runs* is expressed in *h* and the *Volume treated* in $\text{m}^3_{\text{brine}}$. Knowing from the experiments that aeration runs lasted 40 min (0.67 h) and treated 10L (0.01 m^3) of brine:

$$\text{Compressor usage} = \frac{0.67}{0.01} \quad (47)$$

$$\text{Compressor usage} = \mathbf{66.67 \text{ h/m}^3_{\text{brine}}} \quad (48)$$

Knowing that the power of the compressor is 0.75 kW and the average price of electricity in Spain is 0.1 €/kW·h, the energy cost for aeration of brine can be calculated:

$$\text{Aeration cost} = 0.75 \cdot 66.67 \cdot 0.1 \quad (49)$$

$$\text{Aeration cost} = \mathbf{5 \text{ €/m}^3_{\text{brine}}} \quad (50)$$

Finally, the amount of brine treated in the crystallization unit for option iv (CF = 2.75), is calculated as shown in the following equations.

$$\text{Flowrate}_{\text{cryst}} = \frac{\text{Flowrate}_{\text{MD}}}{\text{CF}} \quad (51)$$

$$\text{Flowrate}_{\text{cryst}} = \frac{1584}{2.75} = \mathbf{576 \text{ m}^3/\text{h}} \quad (52)$$

Table 11. Economic evaluation

	Expenses				Revenue				Total	
	Concept	Flowrate (m ³ /h)	Cost (€/m ³)	Expenses (€/h)	Concept	Flowrate (m ³ /h)	Income (€/m ³)	Revenue (€/h)	(€/h)	(€/m ³)
Option i	Discharge	1584	0.078	123.30	Water recovery	0	2.512	0	-123.3	-0.078
Option ii	Crystallization	1584	12.25	19404	Water recovery	1584	2.512	3979.01	-15425	-9.74
Option iii	Acidification	1584	0.32	502.13	Water recovery	1584	2.512	3979.01	-8057.8	-5.09
	MD	1584	1.16	1832.69						
	Crystallization	792	12.25	9702						
Option iv	Acidification	1584	0.32	502.13	Water recovery	1584	2.512	3979.01	-13331.8	-8.42
	Aeration	1584	5	7920						
	MD	1584	1.16	1832.69						
	Crystallization	576	12.25	7056						

Table 11 shows that currently, the most interesting option for brine disposal is its discharge into the sea. This result was expectable and composes one of the major barriers to the development of ZLD technologies. Until fees for discharging brine into natural water bodies become higher, industries will keep on doing it since the alternatives are still too expensive. In this particular case, discharging is two orders of magnitudes cheaper than treating

Crystallization was the most expensive among ZLD options. Even though this technology do not require pretreatment, results suggest that its application should be limited to those streams that cannot be further concentrated in more inexpensive systems (as suggested in options iii and iv). In this regard, MD has the potential to become a cost effective technique for brine concentration. However, the success in the implementation of this method for this particular application necessarily requires inexpensive pretreatments.

By analyzing the results obtained for the two pretreatments selected in the experimental stage, it can be observed that acidification (iii) provides significant saving in OPEX in comparison to acidification followed by aeration (iv). This difference is due to the high cost derived from the compressor. Even though it has not been studied from an economic point of view, aeration followed by acidification would have as well higher OPEX than acidification due to the cost of aeration.

6. Conclusions and recommendations

MD has been proved an effective alternative for RO brine treatment. Throughout experimentation, the DCMD apparatus built for this project has been able to concentrate pretreated brine without showing any kind of flux decrease, yielding an average permeate flux of $9.6 \text{ kg/m}^2 \cdot \text{h}$.

Since MD performance is significantly affected by precipitating salts onto the membrane, salts crystallization must be carried out in a separate stage. Assuming that MD runs on waste heat, its OPEX are one order of magnitude cheaper than those for crystallization. This difference justifies the interest in pretreatments able to delay salts precipitation. The need for pretreatments becomes evident in the case study followed throughout the thesis. RO brine from Sant Joan Despí DWTP is extremely close to the saturation point and therefore it can only be treated by MD after having been pretreated. The components having the highest scaling potential are Ca^{2+} and CO_3^{2-} followed by SO_4^{2-} .

Pretreatment by acidification provides a simple and inexpensive process in which spending 0.32 €/m^3 of brine results in CF as high as 2, i.e. the initial volume can be reduced by 50% before salts start to precipitate. Acidification acts by modifying the equilibrium of the carbonate system and no precipitation occurs during the process. On the other hand, pretreatment by aeration followed by acidification, whose mechanism is the removal of scaling components by precipitation, allows for CF as high as 3 (66% reduction). Even though a higher CF can be achieved by this pretreatment, costs derived from compressor operation make this option economically less attractive than acidification.

Considering this results, acidification would be a better option than aeration followed by acidification. However, further investigation can enhance aeration performance whereas acidification will hardly yield better results due to its mechanism. Acidification only affects the carbonate system; however, there are other components such as SO_4^{2-} that are not affected by this pretreatment. By applying acidification, precipitation of CaCO_3 can be delayed, being CaSO_4 the first precipitating component. However, once this has been achieved (as found in

experimentation), the maximum CF will be determined by CaSO_4 precipitation, and therefore acidification will not further increase the maximum CF.

On the other hand, aeration causes scaling components to precipitate. Even though salts precipitation registered in aeration experiments cannot justify the high costs derived from compressor operation, it is believed that more intensive bubbling conditions could result in higher precipitation of salts. In this regard, it is recommended that further investigation focuses on testing bubbling conditions (i.e. bubble size and distribution), aiming to find suitable operation adjustments that can justify the high OPEX of the compressor.

The two other pretreatment sequences –aeration, and acidification followed by aeration- are not recommended for further experimentation. In the case of aeration, its maximum CF can be doubled just by adding $\sim 0.16 \text{ €/m}^3$ worth of HCl, which makes aeration followed by acidification more interesting. Secondly, acidification followed by aeration cannot compete in terms of OPEX with acidification, and unlike aeration followed by acidification, it cannot be improved with further research because no precipitation occurs in this pretreatment.

Finally, it is worth mentioning that the ZLD systems presented in this thesis have OPEX that can be considered in the same range. However, these OPEX are about 100 times higher than those derived from discharging RO brine from Sant Joan Despí DWTP into the sea.

References

- [1] L. M. Camacho, L. Dumée, J. Zhang, J. De Li, M. Duke, J. Gomez, and S. Gray, “Advances in membrane distillation for water desalination and purification applications,” *Water (Switzerland)*, vol. 5, no. 1, pp. 94–196, 2013.
- [2] Y. Yun, R. Ma, W. Zhang, a. G. Fane, and J. Li, “Direct contact membrane distillation mechanism for high concentration NaCl solutions,” *Desalination*, vol. 188, no. 1–3, pp. 251–262, 2006.
- [3] a. Pérez-González, a. M. Urtiaga, R. Ibáñez, and I. Ortiz, “State of the art and review on the treatment technologies of water reverse osmosis concentrates,” *Water Res.*, vol. 46, no. 2, pp. 267–283, 2012.
- [4] M. Ahmed, W. H. Shayya, D. Hoey, and J. Al-Handaly, “Brine disposal from reverse osmosis desalination plants in Oman and the United Arab Emirates,” *Desalination*, vol. 133, no. 2, pp. 135–147, 2001.
- [5] D. a. Roberts, E. L. Johnston, and N. a. Knott, “Impacts of desalination plant discharges on the marine environment: A critical review of published studies,” *Water Res.*, vol. 44, no. 18, pp. 5117–5128, 2010.
- [6] A. Subramani and J. G. Jacangelo, “Treatment technologies for reverse osmosis concentrate volume minimization: A review,” *Sep. Purif. Technol.*, vol. 122, pp. 472–489, 2014.
- [7] Y. Oren, E. Korngold, N. Daltrophe, R. Messalem, Y. Volkman, L. Aronov, M. Weismann, N. Bouriakov, P. Glueckstern, and J. Gilron, “Pilot studies on high recovery BWRO-EDR for near zero liquid discharge approach,” *Desalination*, vol. 261, no. 3, pp. 321–330, 2010.
- [8] M. S. El-Bourawi, Z. Ding, R. Ma, and M. Khayet, “A framework for better understanding membrane distillation separation process,” *J. Memb. Sci.*, vol. 285, no. 1–2, pp. 4–29, 2006.
- [9] L. Mariah, C. a. Buckley, C. J. Brouckaert, E. Curcio, E. Drioli, D. Jaganyi, and D. Ramjugernath, “Membrane distillation of concentrated brines-Role of water activities in the evaluation of driving force,” *J. Memb. Sci.*, vol. 280, no. 1–2, pp. 937–947, 2006.
- [10] H. Susanto, “Towards practical implementations of membrane distillation,” *Chem. Eng. Process. Process Intensif.*, vol. 50, no. 2, pp. 139–150, 2011.
- [11] M. Gryta, “Fouling in direct contact membrane distillation process,” *J. Memb. Sci.*, vol. 325, no. 1, pp. 383–394, 2008.

- [12] A. Alkudhiri, N. Darwish, and N. Hilal, "Membrane distillation: A comprehensive review," *Desalination*, vol. 287, pp. 2–18, 2012.
- [13] N. Kjellander, "Design and field tests of a membrane distillation system for seawater desalination," *Desalination*, vol. 61, no. 3, pp. 237–243, 1987.
- [14] E. Curcio and E. Drioli, "Membrane Distillation and Related Operations - A Review," *Sep. Purif. Rev.*, vol. 34, no. 1, pp. 35–86, 2005.
- [15] K. Schneider, W. Hölz, R. Wollbeck, and S. Ripperger, "Membranes and modules for transmembrane distillation," *J. Memb. Sci.*, vol. 39, no. 1, pp. 25–42, 1988.
- [16] M. D. Kennedy, J. Kamanyi, S. G. Salinas Rodríguez, N. H. Lee, J. C. Schippers, and G. Amy, "Water Treatment by Microfiltration and Ultrafiltration," *Adv. Membr. Technol. Appl.*, pp. 131–170, 2008.
- [17] F. Banat, N. Jwaied, M. Rommel, J. Koschikowski, and M. Wieghaus, "Desalination by a 'compact SMADES' autonomous solarpowered membrane distillation unit," *Desalination*, vol. 217, no. 1–3, pp. 29–37, 2007.
- [18] D. Winter, J. Koschikowski, and M. Wieghaus, "Desalination using membrane distillation: Experimental studies on full scale spiral wound modules," *J. Memb. Sci.*, vol. 375, no. 1–2, pp. 104–112, 2011.
- [19] K. Lawson and D. Lloyd, "Membrane distillation," *J. Memb. Sci.*, vol. 124, no. 1, pp. 1–25, 1997.
- [20] F. Laganà, G. Barbieri, and E. Drioli, "Direct contact membrane distillation: Modelling and concentration experiments," *J. Memb. Sci.*, vol. 166, no. 1, pp. 1–11, 2000.
- [21] M. Khayet and T. Matsuura, "Preparation and Characterization of Polyvinylidene Fluoride Membranes for Membrane Distillation," *Ind. Eng. Chem. Res.*, vol. 40, no. 24, pp. 5710–5718, 2001.
- [22] M. Khayet, K. Khulbe, and T. Matsuura, "Characterization of membranes for membrane distillation by atomic force microscopy and estimation of their water vapor transfer coefficients in vacuum membrane distillation process," *J. Memb. Sci.*, vol. 238, no. 1–2, pp. 199–211, 2004.
- [23] J. I. Mengual, "Modelling mass transport through a porous partition : Effect of pore size distribution," vol. 29, no. 3, pp. 279–299, 2004.
- [24] L. Martínez, F. J. Florido-Díaz, a. Hernández, and P. Prádanos, "Estimation of vapor transfer coefficient of hydrophobic porous membranes for applications in membrane distillation," *Sep. Purif. Technol.*, vol. 33, no. 1, pp. 45–55, 2003.

- [25] S. Srisurichan, R. Jiratananon, and a. G. Fane, "Mass transfer mechanisms and transport resistances in direct contact membrane distillation process," *J. Memb. Sci.*, vol. 277, no. 1–2, pp. 186–194, 2006.
- [26] a.-S. Jönsson, R. Wimmerstedt, and a.-C. Harrysson, "Membrane distillation - a theoretical study of evaporation through microporous membranes," *Desalination*, vol. 56, pp. 237–249, 1985.
- [27] M. Khayet and T. Matsuura, "Application of surface modifying macromolecules for the preparation of membranes for membrane distillation," *Desalination*, vol. 158, no. 1–3, pp. 51–56, 2003.
- [28] M. Khayet, J. I. Mengual, and T. Matsuura, "Porous hydrophobic/hydrophilic composite membranes: Application in desalination using direct contact membrane distillation," *J. Memb. Sci.*, vol. 252, no. 1–2, pp. 101–113, 2005.
- [29] Y. Wu, Y. Kong, X. Lin, W. Liu, and J. Xu, "Surface-modified hydrophilic membranes in membrane distillation," *J. Memb. Sci.*, vol. 72, no. 2, pp. 189–196, 1992.
- [30] M. Khayet, T. Matsuura, and J. I. Mengual, "Porous hydrophobic/hydrophilic composite membranes: Estimation of the hydrophobic-layer thickness," *J. Memb. Sci.*, vol. 266, no. 1–2, pp. 68–79, 2005.
- [31] a. Bottino, G. Capannelli, and a. Comite, "Novel porous poly (vinylidene fluoride) membranes for membrane distillation," *Desalination*, vol. 183, no. 1–3, pp. 375–382, 2005.
- [32] K. K. Sirkar and Y. Qin, "Novel Membrane and Device for Direct Contact Membrane Distillation Based Desalination Process," no. 87, 2001.
- [33] B. Li and K. K. Sirkar, "Novel membrane and device for vacuum membrane distillation-based desalination process," *J. Memb. Sci.*, vol. 257, no. 1–2, pp. 60–75, 2005.
- [34] C. Gostoli and G. C. Sarti, "Separation of liquid mixtures by membrane distillation," *J. Memb. Sci.*, vol. 41, pp. 211–224, 1989.
- [35] a. C. M. Franken, J. a. M. Nolten, M. H. V. Mulder, D. Bargeman, and C. a. Smolders, "Wetting criteria for the applicability of membrane distillation," *J. Memb. Sci.*, vol. 33, no. 3, pp. 315–328, 1987.
- [36] B. Jiao, a. Cassano, and E. Drioli, "Recent advances on membrane processes for the concentration of fruit juices: A review," *J. Food Eng.*, vol. 63, no. 3, pp. 303–324, 2004.

- [37] J. Zhang, J. D. Li, M. Duke, Z. Xie, and S. Gray, "Performance of asymmetric hollow fibre membranes in membrane distillation under various configurations and vacuum enhancement," *J. Memb. Sci.*, vol. 362, no. 1–2, pp. 517–528, 2010.
- [38] L. F. Dumeé, K. Sears, J. Schuetz, N. Finn, C. Huynh, S. Hawkins, M. Duke, and S. Gray, "Characterization and evaluation of carbon nanotube Bucky-Paper membranes for direct contact membrane distillation," *J. Memb. Sci.*, vol. 351, pp. 36–43 ST – Characterization and evaluation of car, 2010.
- [39] D. E. Suk, T. Matsuura, H. B. Park, and Y. M. Lee, "Development of novel surface modified phase inversion membranes having hydrophobic surface-modifying macromolecule (nSMM) for vacuum membrane distillations," *Desalination*, vol. 261, no. 3, pp. 300–312, 2010.
- [40] D. E. Suk, T. Matsuura, H. B. Park, and Y. M. Lee, "Synthesis of a new type of surface modifying macromolecules (nSMM) and characterization and testing of nSMM blended membranes for membrane distillation," *J. Memb. Sci.*, vol. 277, no. 1–2, pp. 177–185, 2006.
- [41] P. Wang and T. Chung, "Recent advances in membrane distillation processes : Membrane development , configuration design and application exploring," *J. Memb. Sci.*, vol. 474, pp. 39–56, 2015.
- [42] J. Zhang, N. Dow, M. Duke, E. Ostarcevic, J. D. Li, and S. Gray, "Identification of material and physical features of membrane distillation membranes for high performance desalination," *J. Memb. Sci.*, vol. 349, no. 1–2, pp. 295–303, 2010.
- [43] M. Khayet, "Membranes and theoretical modeling of membrane distillation: A review," *Adv. Colloid Interface Sci.*, vol. 164, no. 1–2, pp. 56–88, 2011.
- [44] S. Al-obaidani, E. Curcio, F. Macedonio, G. Di, H. Al-hinai, and E. Drioli, "Potential of membrane distillation in seawater desalination : Thermal efficiency , sensitivity study and cost estimation," vol. 323, pp. 85–98, 2008.
- [45] T. Gullinkala, B. Digman, C. Gorey, R. Hausman, and I. C. E. Æ, "Desalination: Reverse Osmosis and Membrane Distillation," *Sustain. Sci. Eng.*, vol. 2, no. 09, pp. 65–93, 2010.
- [46] Ó. Andrjesdóttir, C. L. Ong, M. Nabavi, S. Paredes, a. S. G. Khalil, B. Michel, and D. Poulidakos, "An experimentally optimized model for heat and mass transfer in direct contact membrane distillation," *Int. J. Heat Mass Transf.*, vol. 66, pp. 855–867, 2013.
- [47] M. N. Chernyshov, G. W. Meindersma, and A. B. de Haan, "Modelling temperature and salt concentration distribution in membrane distillation feed channel," *Desalination*, vol. 157, no. 1–3, pp. 315–324, 2003.

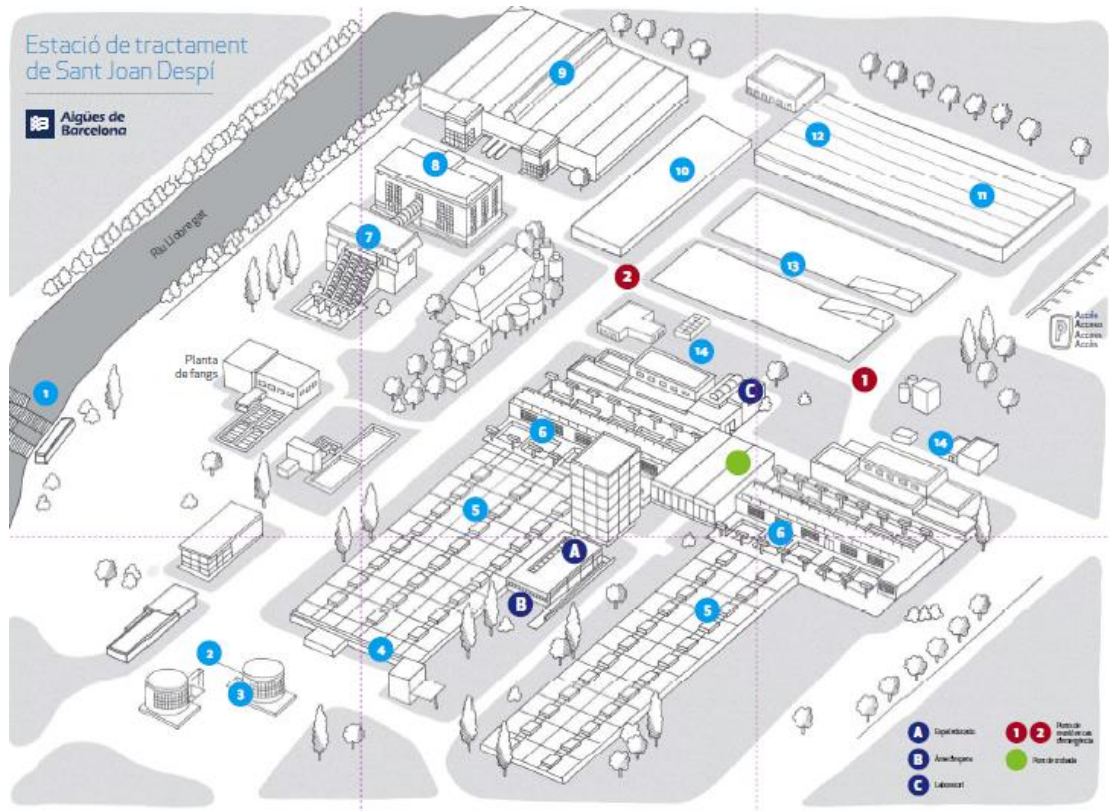
- [48] S. Shirazi, C. J. Lin, and D. Chen, "Inorganic fouling of pressure-driven membrane processes - A critical review," *Desalination*, vol. 250, no. 1, pp. 236–248, 2010.
- [49] C. M. Tun, A. G. Fane, J. T. Matheickal, and R. Sheikholeslami, "Membrane distillation crystallization of concentrated salts—flux and crystal formation," *J. Memb. Sci.*, vol. 257, no. 1–2, pp. 144–155, 2005.
- [50] a. M. Alklaibi and N. Lior, "Membrane-distillation desalination: Status and potential," *Desalination*, vol. 171, no. 2, pp. 111–131, 2005.
- [51] J. Phattaranawik, R. Jiraratananon, and a G. Fane, "Heat transport and membrane distillation coefficients in direct contact membrane distillation," vol. 212, pp. 177–193, 2003.
- [52] M. Khayet, M. P. Godino, and J. I. Mengual, "Thermal boundary layers in sweeping gas membrane distillation processes," *AIChE J.*, vol. 48, no. 7, pp. 1488–1497, 2002.
- [53] K. W. Lawson and D. R. Lloyd, "Membrane distillation. I. Module design and performance evaluation using vacuum membrane distillation," *J. Memb. Sci.*, vol. 120, no. 1, pp. 111–121, 1996.
- [54] L. Martínez-Díez and M. I. Vázquez-González, "A method to evaluate coefficients affecting flux in membrane distillation," *J. Memb. Sci.*, vol. 173, no. 2, pp. 225–234, 2000.
- [55] F. a. Banat and J. Simandl, "Theoretical and experimental study in membrane distillation," *Desalination*, vol. 95, no. 1, pp. 39–52, 1994.
- [56] T. Y. Cath, V. D. Adams, and A. E. Childress, "Experimental study of desalination using direct contact membrane distillation: A new approach to flux enhancement," *J. Memb. Sci.*, vol. 228, no. 1, pp. 5–16, 2004.
- [57] M. Khayet, M. P. Godino, and J. I. Mengual, "Study of Asymmetric Polarization in Direct Contact Membrane Distillation," *Sep. Sci. Technol.*, vol. 39, no. 1, pp. 125–147, 2005.
- [58] M. I. Va, "Temperature and concentration polarization in membrane distillation of aqueous salt solutions," vol. 156, 1999.
- [59] R. W. Schofield, a. G. Fane, C. J. D. Fell, and R. Macoun, "Factors affecting flux in membrane distillation," *Desalination*, vol. 77, pp. 279–294, 1990.
- [60] M. Tomaszewska, M. Gryta, and a. W. Morawski, "The influence of salt in solutions on hydrochloric acid recovery by membrane distillation," *Sep. Purif. Technol.*, vol. 14, no. 1–3, pp. 183–188, 1998.

- [61] a. M. Alklaibi and N. Lior, "Transport analysis of air-gap membrane distillation," *J. Memb. Sci.*, vol. 255, no. 1–2, pp. 239–253, 2005.
- [62] C. Feng, B. Shi, G. Li, and Y. Wu, "Preparation and properties of microporous membrane from for membrane distillation," vol. 237, pp. 15–24, 2004.
- [63] S. Feature, "Pilot plants prove feasibility of a new desalination technique," no. march, pp. 22–26, 2010.
- [64] K. Tarnacki, M. Meneses, T. Melin, J. van Medevoort, and a. Jansen, "Environmental assessment of desalination processes: Reverse osmosis and Memstill?," *Desalination*, vol. 296, pp. 69–80, 2012.
- [65] J. Blanco Gálvez, L. García-Rodríguez, and I. Martín-Mateos, "Seawater desalination by an innovative solar-powered membrane distillation system: the MEDESOL project," *Desalination*, vol. 246, no. 1–3, pp. 567–576, 2009.
- [66] E. Guillén-Burrieza, J. Blanco, G. Zaragoza, D. C. Alarcón, P. Palenzuela, M. Ibarra, and W. Gernjak, "Experimental analysis of an air gap membrane distillation solar desalination pilot system," *J. Memb. Sci.*, vol. 379, no. 1–2, pp. 386–396, 2011.
- [67] A. Kullab and A. Martin, "Membrane distillation and applications for water purification in thermal cogeneration plants," *Sep. Purif. Technol.*, vol. 76, no. 3, pp. 231–237, 2011.
- [68] W. Heinzl, S. Büttner, and G. Lange, "Industrialized modules for MED Desalination with polymer surfaces," *Desalin. Water Treat.*, vol. 42, no. 1–3, pp. 177–180, 2012.
- [69] X. Ji, E. Curcio, S. Al Obaidani, G. Di Profio, E. Fontananova, and E. Drioli, "Membrane distillation-crystallization of seawater reverse osmosis brines," *Sep. Purif. Technol.*, vol. 71, no. 1, pp. 76–82, 2010.
- [70] M. Gryta, "Direct contact membrane distillation with crystallization applied to NaCl solutions," *Chem. Pap. Acad. ...*, no. May 2001, pp. 14–19, 2002.
- [71] D. Lisitsin, D. Hasson, and R. Semiat, "The potential of CO₂ stripping for pretreating brackish and wastewater desalination feeds," *Desalination*, vol. 222, no. 1–3, pp. 50–58, 2008.
- [72] J. Elhajj, M. Al-Hindi, and F. Azizi, "A Review of the Absorption and Desorption Processes of Carbon Dioxide in Water Systems," *Ind. Eng. Chem. Res.*, vol. 53, no. 1, pp. 2–22, 2014.
- [73] W. Stumm and J. J. Morgan, "Aquatic chemistry: chemical equilibria and rates in natural waters," p. 88, 1996.

- [74] K. S. Johnson, "Carbon dioxide hydration and dehydration kinetics in seawater," *Limnology Oceanogr.*, vol. 27, no. 5, pp. 849–855, 1982.
- [75] Y. Cohen and H. Kirchmann, "Increasing the pH of wastewater to high levels with different gases - CO₂ stripping," *Water. Air. Soil Pollut.*, vol. 159, no. 1, pp. 265–275, 2004.
- [76] "No Title," 2009. [Online]. Available: http://braukaiser.com/wiki/index.php?title=File:Carbonic_acid_dissociation.gif. [Accessed: 01-Jul-2015].
- [77] R. Andersson, B. Andersson, F. Chopard, and T. Noren, "Development of a multi-scale simulation method for design of novel multiphase reactors," *Chem. Eng. Sci.*, vol. 59, no. 22–23, pp. 4911–4917, 2004.
- [78] N. de Leeuw and S. Parker, "Surface structure and morphology of calcium carbonate polymorphs calcite, aragonite, and vaterite: An atomistic approach," 1998.
- [79] Catalan Water Agency, "Industrial Uses," 2015. [Online]. Available: http://aca-web.gencat.cat/aca/appmanager/aca/aca.jsessionid=GmLsVzpcPG7rjWThvWvYwWDrfJc pknysS1S97ThWpGSZQ1yjLmnl!742735169!-1073784519?_nfpb=true&_pageLabel=P1215454461208200958970&profileLocale=en. [Accessed: 20-Jun-2015].
- [80] L. F. Greenlee, D. F. Lawler, B. D. Freeman, B. Marrot, and P. Moulin, "Reverse osmosis desalination: Water sources, technology, and today's challenges," *Water Res.*, vol. 43, no. 9, pp. 2317–2348, 2009.
- [81] ACA, "Catalan Water Price Observatory," 2015. [Online]. Available: http://aca-web.gencat.cat/aca/appmanager/aca/aca.jsessionid=dG2JV38f1hg1csj61NckvJL5F6FnTjbnDdpVZmyK9vKcSjSn29ts!-1834914966!1772330541?_nfpb=true&_pageLabel=P19400331401249036779913&profileLocale=en. [Accessed: 20-Jul-2015].
- [82] Bayer MaterialScience Product Center, "Caustic Soda and Hydrochloric Acid," 2014. [Online]. Available: <http://www.materialscience-products.bayer.com/es-ES/Products/Caustic-Soda-and-Hydrochloric-Acid.aspx>. [Accessed: 20-Jul-2015].
- [83] "El precio del ácido clorhídrico sufre una subida del 50% intermensual, debido a la parada de Bayer en Tarragona," *El Confidencial químico*, 2015.
- [84] S. Al-Obaidani and E. Curcio, "Potential of membrane distillation in seawater desalination: thermal efficiency, sensitivity study and cost estimation," *J. Membr. ...*, vol. 167, pp. 327–334, 2008.
- [85] G. Zuo, R. Wang, R. Field, and A. G. Fane, "Energy efficiency evaluation and economic analyses of direct contact membrane distillation system using Aspen Plus," *Desalination*, vol. 283, pp. 237–244, 2011.

Appendix I

Sant Joan Despí DWTP



The drinking water treatment process in the SJD DWTP

1. Catchment: The surface water from the Llobregat is captured using grilles. Under the grilles there are galleries which take the water captured to sand clearing chambers.
2. Sand clearing: The water reaches these sand clearing chambers where the sand and gravel will sediment.

3. First rising: Using submerged pumps we raise the water 11 meters so that it can continue the process by means of gravity.
4. Dosing of reagents and initial disinfection: We add a first dose of chlorine dioxide in order to oxidize inorganic compounds (iron and manganese). We also add the coagulant/flocculant which will cause the agglutination of particles present in the water and their separation by gravity (sedimentation/ decanting).
5. Decanting: The water enters the static decanters where the coagulation and the decanting take place simultaneously. The sludge particles are deposited on the bottom and the clarified water remains in the upper part of the tanks.
6. Sand filtration: We pass the water through sand filters, with a special thickness and grain size, which retain the finer solid particles which may have remained in the water after decanting.
7. Second raising or intermediate pumping: At this point the surface water and the groundwater converge. We raise the water using Archimedes' screws and it is distributed on two independent lines: ozone and activated carbon filtration on one, and ultrafiltration and reverse osmosis with remineralization on the other.
8. Ozonization: Ozone has biocide and oxidant effects. It is mixed with the water in order to remove microorganisms and to oxidize organic matter, favoring its retention in the activated carbon filters.
9. Filtration by granular activated carbon: The aim of this stage is to remove organic compounds, which are absorbed in the granular activated carbon. It also retains metal oxides (iron, manganese, nickel, etc.).
10. Ultrafiltration: Passing the water through the membranes represents a complete barrier against bacteria, but not against viruses. The filtration is necessary for the reverse osmosis membranes to work correctly.
11. Reverse osmosis: Reverse osmosis represents a complete barrier against viruses and bacteria, in addition to removing almost all salts from the water. Passing the water through the three stages of osmosis achieves 90% use of the water and 10% rejection in salts (brine).
12. Remineralization: In order to obtain water with balanced properties, and given that osmosis water is very corrosive, a remineralization is carried out with carbonate rock.
13. Treated water tanks: The water treated with ultrafiltration and osmosis is mixed with the water treated with ozone and granular activated carbon. Chlorine is then dosed in

a first tank, in order to remove the ammonium (pre-chlorination). It then passes to another tank, where the final chlorination is dosed (post-chlorination). This is the dose that guarantees the quality of the water until it reaches the consumption points.

14. Final pumping: Or ending the treatment, the water is pumped from here to the Rellou Plant (Level 50), to Gavà (Level 70) and to the Cornellà Plant (Level 10). From there it goes to other tanks and to all the consumption points.

Sludge treatment (no numbering): In application of the legislation in force, the sludge from the process is treated, so that it becomes a by-product rather than waste. The result is sludge with 95% dryness, which is used as a raw material in construction and other sectors.